J. Fluid Mech. (2019), *vol.* 867, *pp.* 45–76.
doi:10.1017/jfm.2019.128

Investigation of the influence of combustion-induced thermal expansion on two-point turbulence statistics using conditioned structure functions

V. A. Sabelnikov[1,2], A. N. Lipatnikov[3,†], S. Nishiki[4] and T. Hasegawa[5]

[1]Department of Multi-Physics for Energetics, ONERA - The French Aerospace Lab., F-91761 Palaiseau, France

[2]Laboratory of Jet Engine Simulations, Central Aerohydrodynamic Institute (TsAGI), 140180 Zhukovsky, Russian Federation

[3]Department of Mechanics and Maritime Sciences, Chalmers University of Technology, Göteborg 412 96, Sweden

[4]Department of Mechanical Engineering, Kagoshima University, Kagoshima 890-0065, Japan

[5]Institute of Materials and Systems for Sustainability, Nagoya University, Nagoya 464-8603, Japan

(Received 3 April 2018; revised 29 January 2019; accepted 7 February 2019; first published online 20 March 2019)

The second-order structure functions (SFs) of the velocity field, which characterize the velocity difference at two points, are widely used in research into non-reacting turbulent flows. In the present paper, the approach is extended in order to study the influence of combustion-induced thermal expansion on turbulent flow within a premixed flame brush. For this purpose, SFs conditioned to various combinations of mixture states at two different points (reactant–reactant, reactant–product, product–product, etc.) are introduced in the paper and a relevant exact transport equation is derived in the appendix. Subsequently, in order to demonstrate the capabilities of the newly developed approach for advancing the understanding of turbulent reacting flows, the conditioned SFs are extracted from three-dimensional (3-D) direct numerical simulation data obtained from two statistically 1-D planar, fully developed, weakly turbulent, premixed, single-step-chemistry flames characterized by significantly different (7.53 and 2.50) density ratios, with all other things being approximately equal. Obtained results show that the conditioned SFs differ significantly from standard mean SFs and convey a large amount of important information on various local phenomena that stem from the influence of combustion-induced thermal expansion on turbulent flow. In particular, the conditioned SFs not only (i) indicate a number of already known local phenomena discussed in the paper, but also (ii) reveal a less recognized phenomenon such as substantial influence of combustion-induced thermal expansion on turbulence in constant-density unburned reactants and even (iii) allow us to detect a new phenomenon such as the appearance of strong local velocity perturbations (shear layers) within flamelets. Moreover, SFs conditioned to heat-release zones indicate a highly anisotropic influence of combustion-induced thermal expansion on the evolution of small-scale two-point velocity differences within flamelets, with the effects being opposite (an increase or a decrease) for different components of the local velocity vector.

Key words: combustion, flames, turbulent reacting flows

† Email address for correspondence: andrei.lipatnikov@chalmers.se

1. Introduction

The influence of thermal expansion in a premixed turbulent flame on the turbulence characteristics has been investigated by the combustion community over the decades since the seminal work by Karlovitz, Denniston & Wells (1951) and Scurlock & Grover (1953). As reviewed elsewhere (Günther 1983; Bray 1995; Lipatnikov & Chomiak 2010; Sabelnikov & Lipatnikov 2017), the focus of research into the problem was placed on variations in the root-mean-square (r.m.s.) turbulent velocity u' and Reynolds stresses within a mean flame brush, whereas some other important issues were rarely addressed. In particular, a list of such challenging issues includes, but is not limited to (i) the choice of fundamentally justified turbulence characteristics within a premixed flame brush (Lipatnikov 2009), (ii) the influence of combustion-induced thermal expansion on turbulent flow of constant-density unburned reactants within and upstream of a premixed flame brush or (iii) the influence of combustion-induced thermal expansion on two-point flow characteristics, which provide insights into the turbulent kinetic energy distribution over length scales. For instance, spectra of turbulence energy obtained (i) by measuring temporal correlations of velocity fields within premixed flame brushes (Ballal 1979; Gökalp, Shepherd & Cheng 1988; Videto & Santavicca 1990; Furukawa, Okamoto & Hirano 1996; Furukawa, Noguchi & Hirano 2000; Furukawa *et al.* 2002), (ii) by directly extracting two-point spatial correlations of velocity fields from direct numerical simulation (DNS) data (Kolla *et al.* 2014; Lipatnikov *et al.* 2015*b*; Towery *et al.* 2016; O'Brien *et al.* 2017) or (iii) by applying wavelet multi-resolution analysis to DNS data (Kim *et al.* 2018) indicate significant effects of combustion on the spectra, thus, calling for further research into the issue. Due to such effects, it is not yet clear whether or not (or under which conditions) the Kolmogorov (1941) theory may be used to characterize turbulence in flames.

In order to explore the issue more profoundly, the spectral techniques adopted in the papers cited above are worth complementing with a structure function (SF) method, which is widely used by the turbulence community in order to analyse experimental data (Monin & Yaglom 1975; Kuznetsov & Sabelnikov 1990; Frisch 1995; Pope 2000; Davidson 2015) or to develop large eddy simulation (LES) models (Lesieur, Métais & Comte 2005). For instance, Kolmogorov developed his theory of the locally homogeneous and isotropic turbulence by analysing the second-order SFs of the velocity field (Kolmogorov 1941), whereas the famous 5/3 spectrum of turbulence in the inertial subrange was predicted by his PhD student (Obukhov 1941).

However, the SF method has yet been rarely applied to turbulent flames. The present authors are aware of two applications of this method to premixed combustion. Kuznetsov (1982) adopted SFs to model the interaction between turbulence and the hydrodynamic instability (Landau & Lifshitz 1987; Matalon 2007) in premixed flames. Very recently, Whitman *et al.* (2019) numerically investigated SFs that (i) were conditioned to various iso-scalar surfaces in a premixed turbulent flame and (ii) were locally defined in coordinate frameworks centred at various points on each iso-scalar surface. One major goal of the present work, which was mainly done before presentation of the results by Whitman *et al.* (2019), was to develop another conditioned SF method for analysing DNS and experimental data obtained from premixed turbulent flames. Contrary to the study by Whitman *et al.* (2019), the present approach addresses SFs conditioned to the mixture state and defined in the laboratory coordinate framework. Another major goal of the present work was to apply the newly developed method to analysing DNS data in order to advance

understanding of the influence of combustion-induced thermal expansion on turbulence and, in particular, its two-point spatial characteristics.

In the next section, the background to the SF approach is summarized. Subsequently, the approach is extended by introducing conditioned SFs. For this purpose, we will follow ideas developed earlier by Kuznetsov & Sabelnikov (1990) in order to study intermittency in non-reacting turbulent flows. While the extended conditioned SF method can equally well be applied to analysing results of both measurements and simulations, the present work is solely restricted to adapting the method for processing DNS data. Accordingly, the DNS attributes are briefly summarized in the third section. Results obtained by applying the conditioned SF method to analysing the DNS data are discussed in the fourth section followed by conclusions.

2. Structure functions

In the present paper, we restrict ourselves solely to the second-order SFs of velocity field, but the approach can easily be extended to SFs of a higher order.

2.1. *Background*

The second-order SFs of a velocity field are defined as follows (Monin & Yaglom 1975; Pope 2000):

$$D_{ij}(\boldsymbol{r}, \boldsymbol{x}, t) = \langle [u_i(\boldsymbol{x}+\boldsymbol{r}, t) - u_i(\boldsymbol{x}, t)][u_j(\boldsymbol{x}+\boldsymbol{r}, t) - u_j(\boldsymbol{x}, t)] \rangle, \tag{2.1}$$

where t is the time, $\boldsymbol{x}$ and $\boldsymbol{x}+\boldsymbol{r}$ are two spatial points, $r = |\boldsymbol{r}|$ is the distance between them, u_i is the ith component of the velocity vector $\boldsymbol{u}$ and $\langle q \rangle$ designates an ensemble-averaged value of an arbitrary scalar, vector or tensor quantity q. The tensor D_{ij} characterizes the second moments of the velocity difference across scales of size r. Accordingly, D_{ij} measures the energy of such and smaller eddies and, therefore, allows us to examine the energy distribution over the spatial scales directly in the physical space, contrary to energy spectra which deal with wavenumbers. Due to this feature, the second-order SFs are widely used both in theoretical and experimental studies of turbulent flows (Kolmogorov 1941; Monin & Yaglom 1975; Kuznetsov & Sabelnikov 1990; Frisch 1995; Pope 2000; Lesieur *et al.* 2005; Davidson 2015).

In a homogeneous turbulent flow, the tensor D_{ij} does not depend on $\boldsymbol{x}$ and reduces to

$$D_{ij}(\boldsymbol{r}, t) = 2\langle u_i'(\boldsymbol{x}, t) u_j'(\boldsymbol{x}, t) \rangle - R_{ij}(\boldsymbol{r}, t) - R_{ji}(\boldsymbol{r}, t), \tag{2.2}$$

where $q'(\boldsymbol{x}, t) \equiv q(\boldsymbol{x}, t) - \langle q \rangle(t)$ for any scalar, vector or tensor quantity q and

$$R_{ij}(\boldsymbol{r}, t) = R_{ji}(-\boldsymbol{r}, t) = \langle u_i'(\boldsymbol{x}+\boldsymbol{r}, t) u_j'(\boldsymbol{x}, t) \rangle \tag{2.3}$$

are correlation functions (Monin & Yaglom 1975; Pope 2000). Consequently, in a homogeneous turbulent flow, the SFs are directly linked with the correlation functions $R_{ij}(\boldsymbol{r}, t)$, which are used to obtain energy spectra. If the distance r is large when compared to an integral length scale L of the turbulence, then, the correlation functions vanish and $D_{ij} \to 2\langle u_i'(\boldsymbol{x}, t) u_j'(\boldsymbol{x}, t) \rangle$ or $D_{ij} \to 2u'^2 \delta_{ij}$ if the turbulence is not only homogeneous, but also isotropic. Here, δ_{ij} is the Kronecker delta, $u'(t) = \sqrt{u_k'(\boldsymbol{x}, t) u_k'(\boldsymbol{x}, t)/3}$ is the r.m.s. turbulent velocity and the summation convention applies for repeated indexes. In an inhomogeneous turbulent flow, which

is more relevant to combustion, the relationship between the structure and correlation functions is not straightforward. Accordingly, the SFs and energy spectra may convey different (complementary) information in such a case.

In incompressible homogeneous isotropic turbulence (Monin & Yaglom 1975; Pope 2000), the tensor $D_{ij}(\boldsymbol{r}, t)$ is fully determined by a single scalar longitudinal SF

$$D_{LL}(r, t) \equiv \langle [\boldsymbol{u}_L(\boldsymbol{x}+\boldsymbol{r}, t) - \boldsymbol{u}_L(\boldsymbol{x}, t)]^2 \rangle, \tag{2.4}$$

i.e.

$$D_{ij}(\boldsymbol{r}, t) = D_{NN}(r, t)\delta_{ij} + [D_L(r, t) - D_{NN}(r, t)]\frac{r_i r_j}{r^2}, \tag{2.5}$$

with the transverse SF

$$D_{NN}(r, t) \equiv \langle [\boldsymbol{u}_N(\boldsymbol{x}+\boldsymbol{r}, t) - \boldsymbol{u}_N(\boldsymbol{x}, t)]^2 \rangle \tag{2.6}$$

being equal to

$$D_{NN}(r, t) = D_{LL}(r, t) + \frac{r}{2}\frac{\partial D_{LL}}{\partial r}. \tag{2.7}$$

Here, $\boldsymbol{u}_L = \boldsymbol{r}(\boldsymbol{u}\cdot\boldsymbol{r})/r^2$ is the component of the velocity vector $\boldsymbol{u}$ in the direction of vector $\boldsymbol{r}$, and $\boldsymbol{u}_N$ is the component of the velocity vector normal to $\boldsymbol{r}$.

Within the framework of the Kolmogorov theory of the inertial range (Kolmogorov 1941), $D_{LL}(r) = C_2(\langle\varepsilon\rangle r)^{2/3}$ and $D_{NN}(r) = 4D_{LL}(r)/3$, with C_2 being a universal constant. Here, $\varepsilon = 2\nu \mathcal{S}_{ij}\mathcal{S}_{ij}$ is the viscous dissipation rate, ν is the kinematic viscosity of the fluid and $\mathcal{S}_{ij} = 0.5(\partial u_i/\partial x_j + \partial u_j/\partial x_i)$ is the rate-of-strain tensor. Therefore, consistency of DNS conditions with the Kolmogorov theory of turbulence can be checked not only by comparing the energy spectrum with the 5/3 law (Obukhov 1941), as commonly done in combustion DNS, but also by examining (i) in which range of scales l (if any) a ratio of $D_{LL}(r)/(\langle\varepsilon\rangle r)^{2/3}$ or $D_{NN}(r)/(\langle\varepsilon\rangle r)^{2/3}$ is independent of r, (ii) whether or not this range of scales is consistent with $\eta \ll l \ll L$ and (iii) whether or not the computed constant ratio is consistent with the known value of C_2 (or $4C_2/3$, respectively). Here, $\eta = (\nu^3/\langle\varepsilon\rangle)^{1/4}$ is the Kolmogorov length scale.

If r is sufficiently small, e.g. $r \ll \eta$, the two-point velocity difference may be evaluated using Taylor expansion, i.e. $D_{ij} \propto \langle(\partial u_i'/\partial x_k)(\partial u_j'/\partial x_l)\rangle r_k r_l$ in a general case or $D_{LL} \to (\langle\varepsilon\rangle/15\nu)r^2$ in locally homogeneous isotropic turbulence (Kolmogorov 1941).

2.2. *Conditioned structure functions*

Within a premixed turbulent flame brush, local velocity is increased due to a decrease in the local density ρ, caused by combustion-induced thermal expansion. Often, such density changes are localized to thin zones and the local velocity normal to the zone jumps at the burned side of the zone when compared to the unburned side, with such effects being most pronounced in the flamelet regime of premixed turbulent combustion (Bray 1995; Lipatnikov & Chomiak 2010; Sabelnikov & Lipatnikov 2017). Because such a velocity jump is hardly associated with turbulence described by the Kolmogorov theory, the use of mean (ensemble-averaged) quantities for characterizing turbulence in premixed flames appears to be a flawed approach (Lipatnikov 2009; Lipatnikov & Chomiak 2010; Sabelnikov & Lipatnikov 2017), at least in the flamelet

combustion regime. To resolve the problem, flow characteristics conditioned to an unburned (or burned) mixture are often considered instead of mean flow characteristics, as reviewed elsewhere (Lipatnikov & Chomiak 2010). However, as far as energy spectra obtained from spatial correlations computed in DNS are concerned (Kolla *et al.* 2014; Lipatnikov *et al.* 2015*b*; Towery *et al.* 2016; O'Brien *et al.* 2017), the present authors are aware on a single study of the conditioned spectra (Lipatnikov *et al.* 2015*b*), with that study being restricted to the leading edges of mean flame brushes. The SFs offer an opportunity to feel the gap and to gain insight into the conditioned two-point statistics of the turbulent velocity field.

For this purpose, we will follow an approach developed earlier to study intermittency in non-reacting turbulent flows (Kuznetsov & Sabelnikov 1990). Because the aforementioned velocity jump is associated with some kind of intermittency, i.e. unburned–burned intermittency, extension of the approach to premixed flames is straightforward (Sabelnikov *et al.* 2019).

Let us (i) characterize the state of a reacting mixture with a single combustion progress variable $c(\boldsymbol{x}, t)$ (Bray 1995), which monotonically increases from zero in fresh reactants to unity in equilibrium combustion products, and (ii) introduce K indicator functions $I_k(\boldsymbol{x}, t)$, $k = 1, \ldots, K$, such that $I_k(\boldsymbol{x}, t) = 1$ if $c_{k-1} < c(\boldsymbol{x}, t) \leqslant c_k$ and vanishes otherwise. Here, $c_0 = 0$ (fresh) reactants and $c_K = 1$ (equilibrium products). Obviously, the following identity

$$\sum_{k=1}^{K} I_k(\boldsymbol{x}, t) = 1 \tag{2.8}$$

holds at any point at any instant. Then, for any bounded, single-point, scalar, vector or tensor quantity $q(\boldsymbol{x}, t)$,

$$\begin{aligned} \langle q \rangle(\boldsymbol{x}, t) &= \left\langle q(\boldsymbol{x}, t) \sum_{k=1}^{K} I_k(\boldsymbol{x}, t) \right\rangle = \left\langle \sum_{k=1}^{K} q(\boldsymbol{x}, t) I_k(\boldsymbol{x}, t) \right\rangle \\ &= \sum_{k=1}^{K} \langle q(\boldsymbol{x}, t) I_k(\boldsymbol{x}, t) \rangle = \sum_{k=1}^{K} P_k(\boldsymbol{x}, t) \langle q \rangle_k(\boldsymbol{x}, t), \end{aligned} \tag{2.9}$$

and, for any two-point scalar, vector or tensor quantity $Q_{AB} = Q(\boldsymbol{x}_A, \boldsymbol{x}_B, t)$,

$$\langle Q_{AB} \rangle = \left\langle Q_{AB} \left(\sum_{k=1}^{K} I_{A,k} \right) \left(\sum_{l=1}^{K} I_{B,l} \right) \right\rangle = \sum_{k=1}^{K} \sum_{l=1}^{K} \langle Q_{AB} \rangle_{kl} P_{kl}. \tag{2.10}$$

Henceforth, dependencies of various quantities on time t and spatial coordinates $\boldsymbol{x}$ are not specified unless the opposite is required, q_A and q_B designate values of q, measured at points $\boldsymbol{x}_A$ and $\boldsymbol{x}_B = \boldsymbol{x}_A + \boldsymbol{r}$, respectively, at the same instant t, $\langle q \rangle$ is the mean value of q, $\langle q \rangle_k = \langle q I_k \rangle / P_k$ is the value of q conditioned to the kth state of the mixture, i.e. $c_{k-1} < c(\boldsymbol{x}, t) \leqslant c_k$, $P_k(\boldsymbol{x}, t) = \langle I_k \rangle$ is the probability of finding this state at point $\boldsymbol{x}$ at instant t, $\langle Q_{AB} \rangle_{kl} = \langle Q_{AB} I_{A,k} I_{B,l} \rangle / P_{kl}$ is conditioned to the kth state of the mixture at point A and the lth sate of the mixture at point B and $P_{kl} \equiv \langle I_{A,k} I_{B,l} \rangle$ is the probability that the mixture states k and l are recorded at points $\boldsymbol{x}_A$ and $\boldsymbol{x}_B$, respectively, at the same instant.

If Q_{AB} designates tensor $(u_{B,i} - u_{A,i})(u_{B,j} - u_{A,j})$, then, (2.10) reads

$$D_{ij} = \sum_{k=1}^{K} \sum_{l=1}^{K} D_{ij,kl} P_{kl}, \tag{2.11}$$

where subscripts i and j refer to spatial coordinates, subscripts k and l refer to the state of the mixture and

$$D_{ij,kl} \equiv \langle (u_{B,i} - u_{A,i})(u_{B,j} - u_{A,j}) I_{B,l} I_{A,k} \rangle / P_{kl} \tag{2.12}$$

are conditioned SFs.

If $K = 3$, $c_1 = \epsilon \ll 1$ and $c_2 = 1 - \epsilon$, then, there are six different conditioned structure function tensors and six different probabilities:

(i) $D_{ij,11}$ or $D_{ij,uu}$ and P_{11} or P_{uu} (fresh reactants at both points);
(ii) $D_{ij,22}$ or $D_{ij,ff}$ and P_{22} or P_{ff} (intermediate states of the mixture at both points);
(iii) $D_{ij,33}$ or $D_{ij,bb}$ and P_{33} or P_{bb} (equilibrium products at both points);
(iv) $D_{ij,12}$ or $D_{ij,uf}$ and P_{12} or P_{uf} (the reactants at one point, but an intermediate state at another point);
(v) $D_{ij,13}$ or $D_{ij,ub}$ and P_{13} or P_{ub} (the reactants at one point, but the products at another point);
(vi) $D_{ij,23}$ or $D_{ij,fb}$ and P_{23} or P_{fb} (an intermediate state at one point, but the products at another point).

Here, standard subscripts u and b designate unburned (fresh) reactants, i.e. $k = 1$ and $0 \leqslant c(\boldsymbol{x}, t) \leqslant \epsilon$, and burned (equilibrium) products, i.e. $k = 3$ and $1 - \epsilon < c(\boldsymbol{x}, t) \leqslant 1$, whereas intermediate states of the mixture, i.e. $k = 2$ and $\epsilon < c(\boldsymbol{x}, t) \leqslant 1 - \epsilon$, are designated with subscript f associated with flames or flamelets.

Exact transport equations for $D_{ij,kl}$ can be derived using the continuity and Navier–Stokes equations in a general unsteady, inhomogeneous and anisotropic case, as shown in appendix A for $D_{ij,11}$. Since the obtained equation is cumbersome and involves a number of unclosed terms, analysis of it (or transport equations for other conditioned SFs $D_{ij,kl}$) appears to be warranted provided that the capabilities of the newly introduced conditioned SF approach to advance the understanding of turbulent reacting flows is demonstrated. Accordingly, the rest of the paper aims at showing that even simple and direct application of the proposed approach to analysing DNS data can substantially advance our understanding of flame–turbulence interaction. Analysis of the derived transport equation is a subject for future study.

The largest part of the following analysis will be restricted to the aforementioned six conditioned SFs and three states of the mixture. Nevertheless, one more SF tensor $D_{ij,ww}(\boldsymbol{x}, \boldsymbol{r})$ and one more probability $P_{ww}(\boldsymbol{x}, \boldsymbol{r})$, both conditioned to the heat-release zone (HRZ), i.e. to $c_{w,1} < c(\boldsymbol{x}, t) \leqslant c_{w,2}$, will also be addressed in the following. Here, the boundaries of the zone are associated with a threshold value of the rate $W(c)$ of product creation, e.g. $W(c_{w,1}) = W(c_{w,2}) = 0.5 \max\{W(c)\}$, and subscript w indicates a significant reaction rate. Investigation of this SF can shed a new light on the following fundamental issue. Two-dimensional (2-D) DNS study (Poinsot, Veynante & Candel 1991) of the interaction of a laminar premixed flame with a vortex pair and experimental investigations (Roberts *et al.* 1993) of the interaction of a laminar premixed flame with a laminar toroidal vortex have shown that isolated small-scale laminar vortices are inefficient in perturbing the flame HRZ. As reviewed elsewhere (Renard *et al.* 2000; Kadowaki & Hasegawa 2005), this finding was

confirmed in subsequent simulations and measurements of laminar flame–vortex interaction. Accordingly, the smallest-scale turbulent eddies are often hypothesized to be inefficient in stretching HRZs in premixed flames, in particular, because such eddies rapidly disappear due to dilatation and an increase in viscosity within the flame preheat zone. Recent 2-D experimental data by Wabel, Skiba & Driscoll (2018) indicate two trends, i.e. (i) an integral turbulence length scale is increased across flame preheat zones, whereas (ii) the turbulence level does not decrease therein, which (trends) appear to indirectly support the hypothesis (Poinsot *et al.* 1991; Roberts *et al.* 1993; Renard *et al.* 2000; Driscoll 2008) on the disappearance of the smallest-scale turbulent eddies within flame preheat zones. The aforementioned conditioned SF $D_{ij,ww}(\boldsymbol{x}, \boldsymbol{r})$ appears to be perfectly suited to directly exploring the hypothesis.

3. DNS attributes

In the rest of the present paper, we will illustrate certain opportunities associated with the newly introduced conditioned SFs by extracting them from a DNS database created by Nishiki *et al.* (2002, 2006) more than 15 years ago. The choice of this database, which may appear to be outdated when compared to recent DNS data generated in the case of complex combustion chemistry and a high ratio of u' to the laminar flame speed S_L (Aspden, Day & Bell 2016; Lapointe & Blanquart 2016; Uranakara *et al.* 2016; Chaudhuri *et al.* 2017; Wang *et al.* 2017) requires comment.

Since the focus of the following discussion is placed on the influence of combustion-induced thermal expansion on the conditioned SFs of the velocity field, a detailed description of complex combustion chemistry appears to be of secondary importance when compared to two other major requirements. First, it seems to be appropriate to begin a study of any new approach with conditions that are associated with the strongest manifestation of the effects the approach aims at. Accordingly, in order to make the thermal expansion effects as strong as possible, the heat release and density drop should be localized to sufficiently thin zones and the velocity jump across such zones should be sufficiently large when compared to u'. In other words, the flamelet regime of premixed turbulent combustion associated with a low ratio of u'/S_L should be addressed. The DNS by Nishiki *et al.* (2002, 2006) did deal with this regime, as discussed in detail by Lipatnikov, Nishiki & Hasegawa (2015*c*), whereas the vast majority of recent very advanced DNS studies attacked other combustion regimes. Second, to better explore the thermal-expansion effects, data obtained at significantly different density ratios $\sigma = \rho_u/\rho_b$ are required and the DNS database by Nishiki *et al.* (2002, 2006) does satisfy this requirement, because cases of $\sigma = 2.5$ and 7.53 were simulated, with all other things being roughly equal. Third, the major goal of the present work consists in introducing conditioned SFs and showing the opportunities offered by this new method for analysing DNS and experimental data, rather than scrutinizing particular local effects. The selected DNS data appear to be fully adequate to this major goal, because they allow us to quickly calculate and analyse a large amount of results of significantly different types.

Since the DNS data were discussed in detail elsewhere (Nishiki *et al.* 2002, 2006) and were already used by various research groups (Im *et al.* 2004; Mura, Tsuboi & Hasegawa 2008; Mura *et al.* 2009; Robin *et al.* 2010; Bray *et al.* 2011; Robin, Mura & Champion 2011; Lipatnikov, Nishiki & Hasegawa 2014; Lipatnikov *et al.* 2015*a*,*c*,*d*, 2017, 2018*a*,*b*,*c*,*d*; Sabelnikov *et al.* 2016, 2017, 2019; Lipatnikov, Nishiki & Hasegawa 2019), we will restrict ourselves to a brief summary of those

compressible 3-D simulations. They dealt with statistically planar, 1-D, equidiffusive, adiabatic flames modelled by unsteady 3-D continuity, Navier–Stokes and energy equations, supplemented with a transport equation for the mass fraction Y of a deficient reactant and the ideal gas state equation. The Lewis and Prandtl numbers were equal to 1.0 and 0.7, respectively. Combustion chemistry was reduced to a single reaction. Accordingly, the mixture state was completely characterized by a single combustion progress variable $c = 1 - Y/Y_u$. Temperature dependence of the molecular transport coefficients was taken into account, e.g. $\nu = \nu_u(T/T_u)^{0.7}$.

The computational domain was a rectangular box $\Lambda_x \times \Lambda_y \times \Lambda_z$ with $\Lambda_x = 8$ mm, $\Lambda_y = \Lambda_z = 4$ mm, and was resolved using a uniform rectangular ($2\Delta x = \Delta y = \Delta z$) mesh of $512 \times 128 \times 128$ points. Homogeneous isotropic turbulence ($u' = 0.53$ m s^{-1}, $L = 3.5$ mm, $\eta = 0.14$ mm and the turbulent Reynolds number $Re_t = u'L/\nu_u = 96$ (Nishiki *et al.* 2002, 2006)) was generated in a separate box and was injected into the computational domain through the left boundary $x = 0$. In the computational domain, the turbulence decayed along the direction x of the mean flow. The flow was periodic in the y and z directions.

At $t = 0$, a planar laminar flame was embedded into statistically the same turbulence assigned for the velocity field in the entire computational domain. Subsequently, the inflow velocity was increased twice, i.e. $U(0 \leqslant t < t_I) = S_L < U(t_I \leqslant t < t_{II}) < U(t_{II} \leqslant t)$, in order to keep the flame in the computational domain until the end t_{III} of the simulations.

Three cases H, M and L characterized by high, medium, and low, respectively, density ratios were studied (Nishiki *et al.* 2002, 2006). Since the focus of the present work is placed on thermal-expansion effects, the following discussion will be restricted to a comparison of the results obtained in the two cases characterized by the highest and the lowest density ratios, i.e. (i) case H characterized by the highest $\sigma = 7.53$, $S_L = 0.6$ m s^{-1}, $\delta_L = 0.217$ mm, $Da = 18$, $Ka = 0.21$, $S_t = 1.15$ m s^{-1}, and (ii) case L characterized by the lowest $\sigma = 2.5$, $S_L = 0.416$ m s^{-1}, $\delta_L = 0.158$ mm, $Da = 17.3$, $Ka = 0.30$ and $S_t = 0.79$ m s^{-1}. Here, $\delta_L = (T_b - T_u)/\max\{|\nabla T|\}$ is the laminar flame thickness, $Da = (L/u')/(\delta_L/S_L)$ and $Ka = (u'/S_L)^{3/2}(L/\delta_L)^{-1/2}$ are the Damköhler and Karlovitz numbers, respectively, evaluated at the leading edges of the mean flame brushes. The two flames are well associated with the flamelet combustion regime, e.g. various Bray–Moss–Libby (BML) expressions hold in cases H and L (Lipatnikov *et al.* 2015*c*, figures 1–4).

The DNS data were processed as follows. Mean quantities $\langle q \rangle(x)$ were averaged over transverse yz-planes and over time $t_{II} \leqslant t \leqslant t_{III}$ (220 and 200 snapshots in cases H and L, respectively, stored during a time interval of $t_{III} - t_{II} \approx 1.5L/u' \approx 10$ ms). Subsequently, x-dependencies were mapped to $\langle c \rangle$-dependencies using the spatial profiles of the Reynolds-averaged combustion progress variable $\langle c \rangle = 1 - \langle Y \rangle / Y_u$, i.e. the mean value $\langle q \rangle(x)$ was linked with the mean value $\langle c \rangle(x)$ of the combustion progress variable. Accordingly, in the following, dependencies of $\langle q \rangle(x)$ and $\langle c \rangle(x)$ extracted directly from the DNS data will be presented in the form of $\langle q \rangle(\langle c \rangle)$ or $\langle q \rangle[\langle c \rangle(x)]$. The probabilities $P_{kl}[\langle c \rangle(x), r]$ were also extracted from the DNS data, with reactants and products being associated with $c(\boldsymbol{x}, t) \leqslant \epsilon$ and $c(\boldsymbol{x}, t) > 1 - \epsilon$, respectively. Change of the threshold ϵ from 0.05 to 0.01 did not affect the major results reported in the following. Therefore, we will restrict ourselves to reporting data computed at $\epsilon = 0.05$.

The flow in the flame H or L is statistically homogeneous and isotropic in any transverse plane $x = \text{const.}$, but the axial flow $u(\boldsymbol{x}, t)$ is accelerated by the mean axial pressure gradient $\partial \langle p \rangle / \partial x$ induced due to combustion. Therefore, to distinguish

spatial variability of the turbulent flow from the pressure-driven acceleration of the flow, the focus of the following discussion is placed on SFs measured at two points $\boldsymbol{x}_A = \{x_{AB}, y_A, z_A\}$ and $\boldsymbol{x}_B = \{x_{AB}, y_B, z_B\}$ that lie on the same transverse plane $x = x_{AB}$, i.e. $\boldsymbol{r} = \{0, r_y, r_z\}$, $r_y = y_B - y_A$ and $r_z = z_B - z_A$. Nevertheless, some results obtained for $\boldsymbol{r} = \{r, 0, 0\}$, i.e. $\boldsymbol{x}_B = \boldsymbol{x}_A + r$, $y_B = y_A$ and $z_B = z_A$, will also be reported in § 4.3.

For the axial velocity u, the transverse SFs $D_{xx,T}[\langle c\rangle(x), r]$ and their conditioned components were obtained by (conditionally) averaging $(u_B - u_A)^2$ over time and two sets of points; (i) $\boldsymbol{x}_A = \{x, y, z\}$, $\boldsymbol{x}_B = \{x, y + r, z\}$ and (ii) $\boldsymbol{x}_A = \{x, y, z\}$, $\boldsymbol{x}_B = \{x, y, z + r\}$. It is worth noting that, following Kolmogorov (1941), the words 'transverse' and 'longitudinal' SF or subscripts T and L, respectively, characterize the mutual orientation of velocity vector $\boldsymbol{u}(\boldsymbol{x}, t)$ or $\boldsymbol{u}(\boldsymbol{x} + \boldsymbol{r}, t)$ and vector $\boldsymbol{r}$ that connects the two considered points. The longitudinal and transverse SFs should be distinguished from the axial (x) and transverse (y or z) directions, which are normal and tangential, respectively, to the mean flame brush. For instance, the longitudinal SF for tangential velocity v or w characterizes variations in that velocity in the transverse direction y or z, respectively. For the tangential velocities v and z, the transverse SFs $D_{yy,T}[\langle c\rangle(x), r]$ and $D_{zz,T}[\langle c\rangle(x), r]$, respectively, and their conditioned components were obtained by (conditionally) averaging $(v_B - v_A)^2$ and $(w_B - w_A)^2$, respectively, over time and sets of points (ii) and (i), respectively. On the contrary, the longitudinal tangential velocity SFs $D_{yy,L}[\langle c\rangle(x), r]$ and $D_{zz,L}[\langle c\rangle(x), r]$ and their conditioned components were obtained by (conditionally) averaging $(v_B - v_A)^2$ and $(w_B - w_A)^2$, respectively, over time and sets of points (i) and (ii), respectively. Finally, SFs $D_{yz,T}[\langle c\rangle(x), r] = 0.5(D_{yy,T} + D_{zz,T})$ and $D_{yz,L}[\langle c\rangle(x), r] = 0.5(D_{yy,L} + D_{zz,L})$ were found. Here, $\boldsymbol{u} = \{u, v, w\}$, $0 \leqslant y < \Lambda_y$, $0 \leqslant z < \Lambda_z$ and $0 \leqslant r < \Lambda_y/2 = \Lambda_z/2$.

4. Results and discussion

4.1. *Typical structure functions*

Typical mean (dots) and conditioned (lines) SFs are shown in figures 1–3. These data were computed in the middle of the flame brushes, i.e. at distance x^* characterized by the minimal difference $|\langle c\rangle(x) - 0.5|$, in order for the probabilities $P_{kl}(\langle c\rangle, r)$ to be significant, see figure 4, thus, allowing us to obtain solid statistics. The SFs are normalized using the square $|\Delta u|_L^2$ of the normal velocity jump $|\Delta u|_L = (\sigma - 1)S_L$ across the laminar flame ($|\Delta u|_L^2 = 15.35$ and $0.39\ \mathrm{m^2\ s^{-2}}$ in cases H and L, respectively). The distance r is normalized using the distance δ_ϵ between iso-surfaces $c = \epsilon$ and $c = 1 - \epsilon$ in the unperturbed laminar flame ($\delta_\epsilon = 0.28$ and 0.22 mm in cases H and L, respectively). This distance is used instead of δ_L, because reactant–product SFs should vanish if $r < \delta_\epsilon$ provided that the flamelets retain the local structure of the unperturbed laminar flame. The laminar flame scales are chosen, because a substantial part of subsequent discussion, e.g. see § 4.2, will address the behaviour of reactant–product SFs at distances close to δ_ϵ.

To illustrate the capabilities of the SF approach, let us note certain trends indicated in figures 1–3.

First, the mean SFs differ substantially from the conditioned SFs, thus, showing that the velocity jumps associated with the unburned–burned intermittency strongly change the two-point statistics of the velocity field within a premixed turbulent flame brush. Therefore, the results plotted in figures 1–3 call for investigation of the conditioned fields in order to properly characterize the aforementioned two-point statistics.

Second, the magnitudes of almost all SFs are significantly increased by the density ratio σ, cf. results obtained in cases H and L. (The higher magnitude of reactant–reactant (i.e. *uu*) SFs computed in case H is associated with a shorter time during

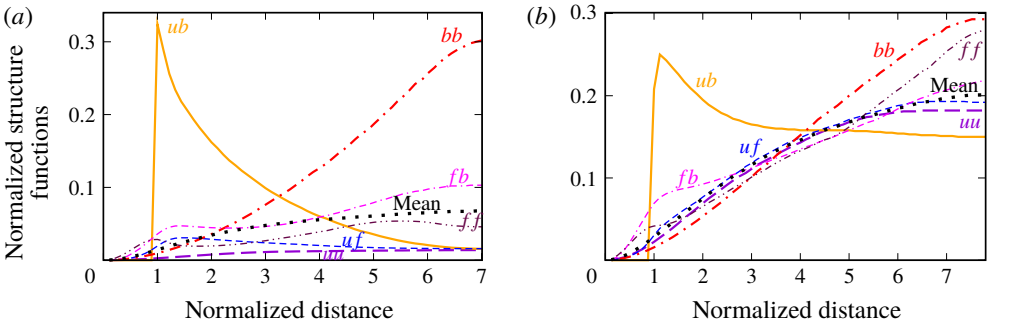

FIGURE 1. (Colour online) Normalized conditioned (lines) and mean (dots) longitudinal SFs $D_{yz,L}[\langle c\rangle(x^*), r/\delta_\epsilon]/|\Delta u|_L^2$ for the transverse velocity, obtained in the middle of flame brush in case (*a*) H or (*b*) L.

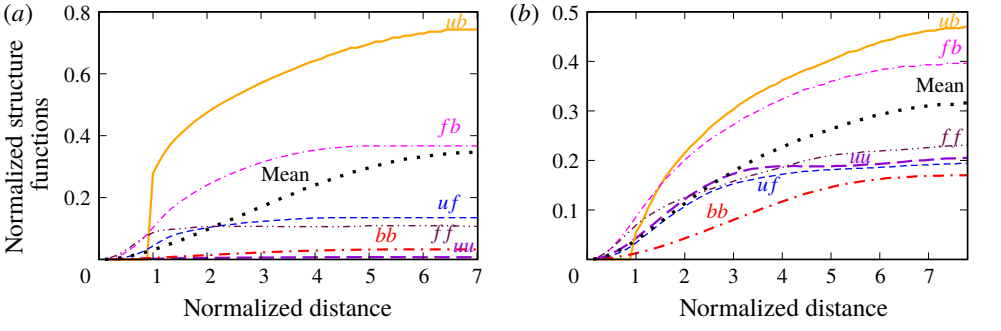

FIGURE 2. (Colour online) Normalized conditioned (lines) and mean (dots) transverse SFs $D_{xx,T}[\langle c\rangle(x^*), r/\delta_\epsilon]/|\Delta u|_L^2$ for the axial velocity, obtained in the middle of flame brush in case (*a*) H or (*b*) L.

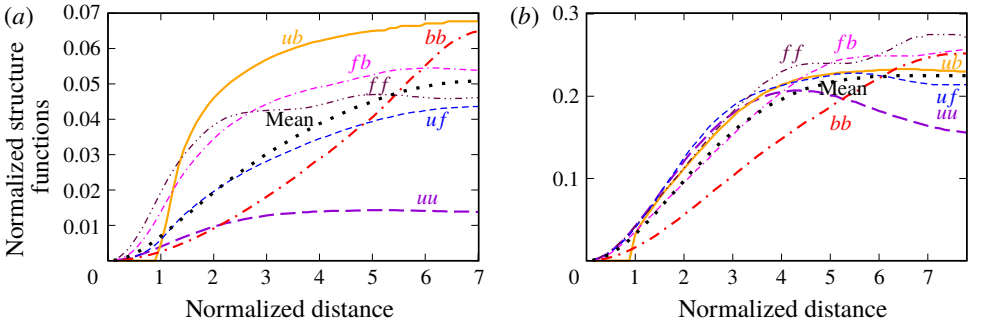

FIGURE 3. (Colour online) Normalized conditioned (lines) and mean (dots) transverse SFs $D_{yz,T}[\langle c\rangle(x^*), r/\delta_\epsilon]/|\Delta u|_L^2$ for the transverse velocity, obtained in the middle of flame brush in case (*a*) H or (*b*) L.

which the turbulence decays upstream of the mean flame brush, as discussed in detail elsewhere (Lipatnikov *et al.* 2018*a*). This time is shorter in case H when compared to case L, because the turbulent flame speed S_t and the mean inlet velocity are higher

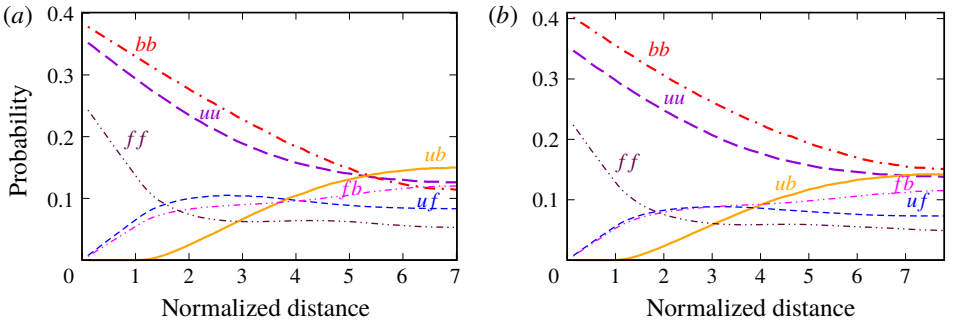

FIGURE 4. (Colour online) Probabilities $P_{kl}[\langle c\rangle(x^*), r/\delta_\epsilon]$ obtained in the middle of flame brush in case (*a*) H or (*b*) L.

in the former case, whereas distances from the inlet to the flame leading edges are approximately equal in the two cases.) This trend is expected because variations in the density increase the variability of the velocity field and, consequently, the velocity differences between two points. The discussed difference between cases H and L is much more pronounced if different mixture states are observed at the two points, i.e. if the difference in ρ_A and ρ_B is large, cf. curves *ub*, *uf* or *fb* in cases H and L.

Third, in case H, the reactant–reactant SFs, see curves *uu* plotted by the dashed lines in figures 1(*a*) and 2(*a*), have the lowest magnitudes among all conditioned SFs, because the reactants are least subjected to thermal-expansion effects.

Fourth, curves *ub* plotted by the solid lines in figure 2 show that the transverse reactant–product SF $D_{xx,T,ub}$ for the axial velocity has the largest magnitude among all SFs plotted in figures 1–3, with the effect being much more pronounced in case H. These trends are associated with strong (weak) axial acceleration of low-density products (high-density reactants) by the combustion-induced mean axial pressure gradient $\langle \nabla_x p\rangle$, which is significantly stronger in case H. In particular, an increase in the reactant–product SF $D_{xx,T,ub}$ with distance r may be attributed to a mechanism highlighted by Scurlock & Grover (1953) and by Libby & Bray (1981). For instance, if the reactant coordinate $\boldsymbol{x}_A$ is kept constant, but the distance r is increased, the axial distance between low-density products at point B and the flamelet surface is likely to be increased. Therefore, the products have strongly been accelerated by $\rho^{-1}\langle \nabla_x p\rangle$ during a longer time required to reach a more distant point B. Consequently, their axial velocity is higher at that point.

Fifth, a decrease in the longitudinal reactant–product SF $D_{yz,L,ub}$ with r, see curves *ub* plotted by the solid lines in figure 1, may be attributed to the same mechanism bearing in mind that the studied flames generate a mean axial pressure gradient $\langle \nabla_x p\rangle$, but do not induce a mean transverse pressure gradient. Accordingly, when the products are accelerated by $\langle \nabla_x p\rangle$ in the axial direction, the magnitude of their transverse velocity decreases due to mass conservation, because the product density is constant.

Sixth, as discussed in detail elsewhere (Lipatnikov *et al.* 2015*c*), the local flamelet structure is weakly perturbed (when compared to the laminar flame) under conditions of the present DNS at $\langle c\rangle(x^*) \approx 0.5$. Therefore, reactants and products cannot simultaneously be observed at two points separated by a distance r that is substantially less than δ_ϵ. Accordingly, the probability P_{ub} vanishes if $r/\delta_\epsilon < 1$, see curves *ub* plotted by the solid lines in figure 4. Nevertheless, at $r/\delta_\epsilon \approx 1$, the probability

is small, but finite, and there is a jump of the longitudinal reactant–product SF $D_{yz,L,ub}$, see curves *ub* plotted by the solid lines in figure 1. This jump is attributed to local flow acceleration across flamelets in the directions that are locally normal to the flamelets. The location of the jump at $r/\delta_\epsilon \approx 1$ indicates the appearance of flamelets that are locally normal to the y or z coordinate axis. Indeed, if a flamelet is significantly inclined to both transverse axes, the distance between the reactant and product edges of the flamelet, counted in the y or z direction, is larger than the distance δ_ϵ counted between the two edges in the locally normal direction.

Seventh, a significant increase in the longitudinal product–product SF $D_{yz,L,bb}$ with r observed in case H, see curve *bb* plotted by the dotted-dashed line in figure 1(*a*), might result from the opposite directions of the transverse velocities v (or w) induced due to thermal expansion at opposite sides of a layer that is filled by the reactants and is almost parallel to the x-axis. Such finger-like structures were observed by analysing the present DNS data (Lipatnikov *et al.* 2015*a*, 2018*a*). In case L, an increase in the longitudinal product–product SF $D_{yz,L,bb}$ with r is also observed, but the magnitude of the effect is much lower due to significantly weaker flow acceleration within flamelets.

Eighth, the transverse flamelet–product $D_{xx,T,fb}$ and reactant–flamelet $D_{xx,T,uf}$ SFs behave similarly to the reactant–product SF $D_{xx,T,ub}$, cf. curves *fb*, *uf* and *ub*, respectively, in figure 2, but have smaller magnitudes, because the density difference is largest for the reactant–product pairs of points.

Ninth, differences between SFs conditioned to various events are smallest in the case of SF $D_{yz,T}$, because $\langle \nabla_y p \rangle = \langle \nabla_z p \rangle = 0$ and flamelets normal to the y (or z) component of the local velocity field do not induce a pressure gradient in the transverse z (or y, respectively) direction. Accordingly, the influence of combustion on the SFs is least pronounced for the transverse SF $D_{yz,T}$ for the tangential velocities v and w in the selected coordinate framework.

Thus, the considered examples show that (i) the conditioned SFs convey a large amount of information on the influence of combustion-induced thermal expansion on velocity fields in premixed turbulent flames and (ii) this influence is significantly reduced when the density ratio is decreased. Although the trends discussed above might be claimed to be expected, the use of the SFs offers an opportunity to reveal an apparently surprising effect examined in the next subsection.

4.2. *Local shear layers*

Figures 1–3 show that the reactant–product SFs vanish at $r/\delta_\epsilon < 1$, but have finite or even peak values close to $r/\delta_\epsilon = 1$. Thus, if $r > \delta_\epsilon$, then, independently of a transverse direction (y or z), there are pairs of points $(\boldsymbol{x}_A, \boldsymbol{x}_B)$ such that (i) both points lie on a line parallel to a transverse coordinate axis, (ii) distance r between the two points is close to δ_ϵ and (iii) $c(\boldsymbol{x}_A, t) < 0.05$ and $c(\boldsymbol{x}_B, t) > 0.95$ or *vice versa*. However, the probability of such events is low if r is close to δ_ϵ, see solid line in figure 4. As already argued in the previous subsection, such events are associated with flamelets that are locally normal to a transverse coordinate axis y or z.

Moreover, at the lowest $r \approx \delta_\epsilon$ associated with a finite probability $P_{ub} > 0$, the normalized reactant–product SF $D_{yz,T,ub}/|\Delta u|_L^2$ has a very small magnitude of approximately 0.05 at $\langle c \rangle = 0.5$ in case H. If flamelets that control the SF at $r \approx \delta_\epsilon$ were inclined to both transverse axes y and z, then, contributions from $D_{yy,T,ub}$, i.e. difference in v in the z-direction, and from $D_{zz,T,ub}$, i.e. difference in w in the y-direction, would yield a significantly larger $D_{yz,T,ub}/|\Delta u|_L^2$ due to jumps of the locally normal components of v and w across the flamelets. Consequently, the computed small

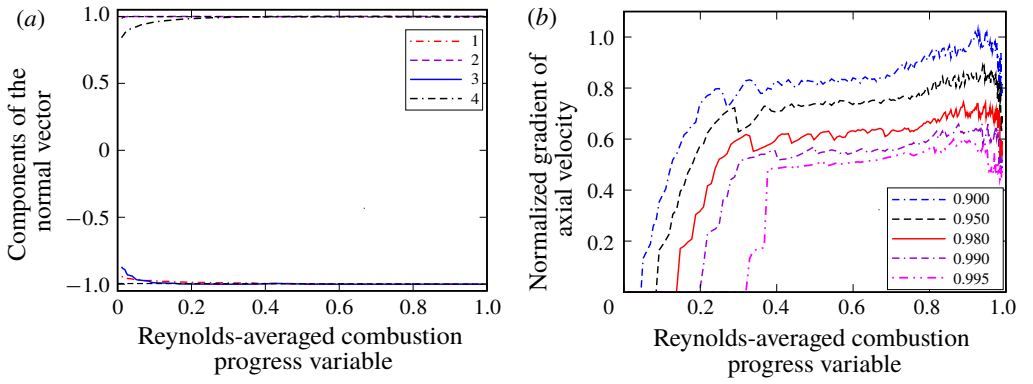

FIGURE 5. (Colour online) (*a*) Minimal and maximal values of the transverse components of the unit normal vector $\boldsymbol{n} = -\nabla c/|\nabla c|$, found for each transverse plane $\langle c\rangle(x) =$ const. and various instants t. 1 – $\min\{n_y\}$, 2 – $\max\{n_y\}$, 3 – $\min\{n_z\}$, 4 – $\max\{n_z\}$. (*b*) Maximal (over each transverse plane at various instants) absolute values $|\langle \boldsymbol{n}\cdot\nabla u|\sqrt{n_y n_y} > n^*\|\sqrt{n_z n_z} > n^*\rangle|$ of the normal (to the local flamelet) gradient of the axial velocity u conditioned to either $|n_y|$ or $|n_z|$ being larger than a threshold value n^* specified in the legends. The gradient is normalized using the magnitude $|\nabla u|_L = (\sigma - 1)S_L/\delta_L$ of the velocity gradient across the laminar flame. Case H.

magnitude of $D_{yz,T,ub}/|\Delta u|_L^2$ at $r \approx \delta_\epsilon$ also indicates that flamelets associated with the lowest distance r_y or r_z between the reactants and products are almost normal to the y or z-axis, respectively.

Nevertheless, the peak value of $D_{yz,L,ub}[\langle c\rangle(x^*), r/\delta_\epsilon]$, obtained at $r \approx \delta_\epsilon$, see curve *ub* in figure 1(*a*), and, therefore, controlled by such 'locally normal' (to the y or z-axis) flamelets, is substantially less than $|\Delta u|_L^2$. This result implies that the local velocity field within such flamelets is significantly perturbed when compared to the velocity field within the laminar flame.

Furthermore, the magnitude of $D_{xx,T,ub}/|\Delta u|_L^2$ at $r \approx \delta_\epsilon$ in case H, see curve *ub* in figure 2, is as large as 0.28 and is comparable with $D_{yz,L,ub}/|\Delta u|_L^2 = 0.32$ at the same r/δ_ϵ. This result implies that there are significant variations in the axial velocity u across the considered flamelets, to which the velocity is almost tangential.

Thus, the discussed behaviour of the reactant–product SFs implies (i) appearance of flamelets almost normal to the y or z-axis, (ii) strong perturbations of the local velocity field within such flamelets (when compared to the laminar flame) and, in particular, (iii) strong variations in the locally tangential (to the flamelets) velocity u in the direction locally normal to the flamelets.

Since the present authors are not aware of any discussion of such local flow structures in the combustion literature, target-directed diagnostics were applied to the same DNS data in order to validate the above conclusions drawn by analysing the conditioned SFs. In the following, we will restrict ourselves to reporting some results that support the aforementioned effects revealed using the conditioned SFs. The reader interested in a more detailed discussion of these effects is referred to a paper by Lipatnikov *et al.* (2018*c*).

Figure 5(*a*) shows that the maximal (minimal) values of the transverse components n_y and n_z of the unit normal vector $\boldsymbol{n} = -\nabla c/|\nabla c|$, found for each transverse plane $\langle c\rangle(x) =$ const. at various instants, are very close to unity (minus unity) provided

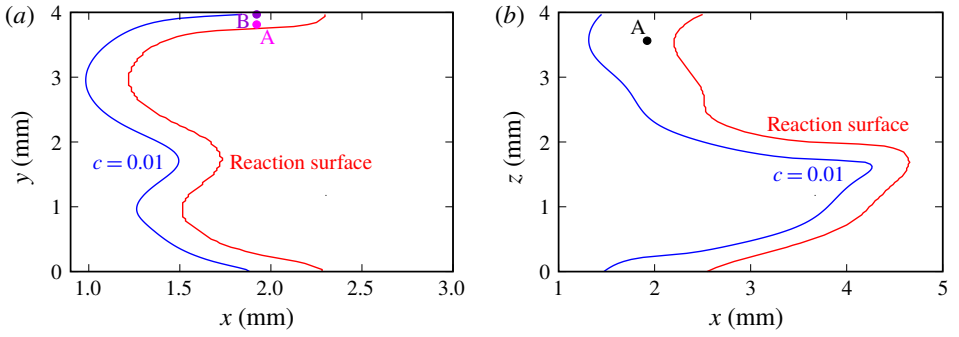

FIGURE 6. (Colour online) Flame shapes in (*a*) *xy* and (*b*) *xz* planes that cross a point A characterized by $n_y \approx 1$ and by a high magnitude $|\boldsymbol{n} \cdot \nabla u|$ of the normal (to the local flamelet) gradient of the axial velocity u, which is almost tangential to the flamelet in the vicinity of that point. Reaction surface is characterized by the maximal reaction rate $W(c)$. $\langle c \rangle (x^*) \approx 0.5$. Case H, $t = 18.3$ ms.

that $\langle c \rangle (x) \geqslant 0.2$. Consequently, $|n_y|$ (or $|n_z|$) is very close to unity at some (or another) point (y, z) for each x such that $\langle c \rangle (x) \geqslant 0.2$ at some (or another) instant. Accordingly, at such points and at such instants, $|n_x| = \sqrt{1 - n_y^2 - n_z^2} \ll 1$ and flamelets locally parallel to the x-axis do appear, in line with the above discussion of the reactant–product SFs. An example of such a flamelet is shown in the upper part of figure 6(*a*), see the neighbourhood of point A therein.

Figure 5(*b*) indicates that the locally tangential (to such flamelets) velocity u can significantly vary in the direction locally normal to the flamelets, in line with the above discussion, but contrary to the behaviour of the velocity field in weakly stretched laminar flames. Such variations of u in the y-direction are shown by the dotted line in figure 7(*a*).

Insight into a physical mechanism that can cause such a large locally normal gradient $|\boldsymbol{n} \cdot \nabla u|$ of the locally tangential velocity u can be gained by looking into figures 6(*a*), 7 and 8. At point A, which is close to the reaction surface characterized by the maximal reaction rate as shown in figure 6(*a*), $n_y \approx 1$, whereas $|n_x| \ll 1$ and $|n_z| \ll 1$. Accordingly, in the vicinity of point A, the reaction surface is almost parallel to the x-axis and the axial distance Δx between point A and the flamelet cold boundary $c(x, y_A, z_A, t) = 0.01$ is relatively large ($\Delta x_A = 0.6$ mm). On the contrary, a neighbouring point B ($x_B = x_A$, $y_B = y_A + r$ and $z_B = z_A$) is close to the cold boundary ($\Delta x_B = 0.07$ mm). Consequently, a fluid volume that comes to point A is likely to move within the flamelet during a time interval Δt_A, which is significantly longer than the time interval Δt_B required for another fluid volume to move from the flamelet cold boundary to point B. When a fluid volume moves within the flamelet, the density in the volume is less than ρ_u and decreases with distance from the flamelet cold boundary. Therefore, the volume acceleration $\rho^{-1} \nabla p$ by the combustion-induced pressure gradient is significantly stronger than the acceleration that a volume of unburned reactants would experience under the influence of the same pressure gradient, cf. solid and dotted-dashed lines in figure 7(*b*) or see figure 8(*b*). Thus, the volume associated with point A (or B) is subject to an increased axial acceleration, see solid line in figure 7(*a*) or figure 8(*a*), during a relatively long (short, respectively) time interval Δt_A (Δt_B, respectively). As a result, a significant

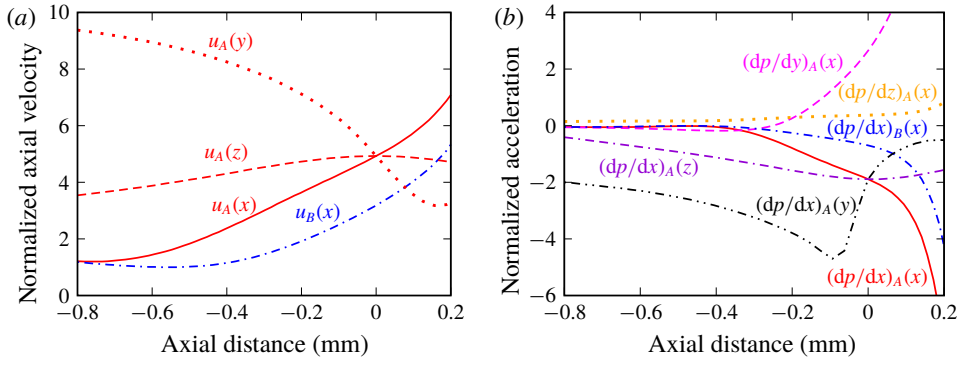

FIGURE 7. (Colour online) Local profiles of (*a*) the *x*-component $u(\boldsymbol{x})$ of the velocity vector $\boldsymbol{u} = \{u, v, w\}$ and (*b*) components of the pressure-induced acceleration vector $\rho^{-1}\boldsymbol{\nabla} p$. Axial profiles plotted by dotted-dashed lines cross point B shown in figure 6(*a*), with the axial distance being counted from the transverse plane $z = z_A$ that points B and A lie on. Other profiles cross point A shown in figure 6, with distance being counted from this point. Negative distance is associated with lower (or higher) values of the combustion progress variable c for the x and z (or y, respectively) profiles. The velocity is normalized using S_L, the density is normalized using ρ_u, and the pressure gradient is normalized using $\rho_u(\sigma - 1)S_L^2/\delta_L$.

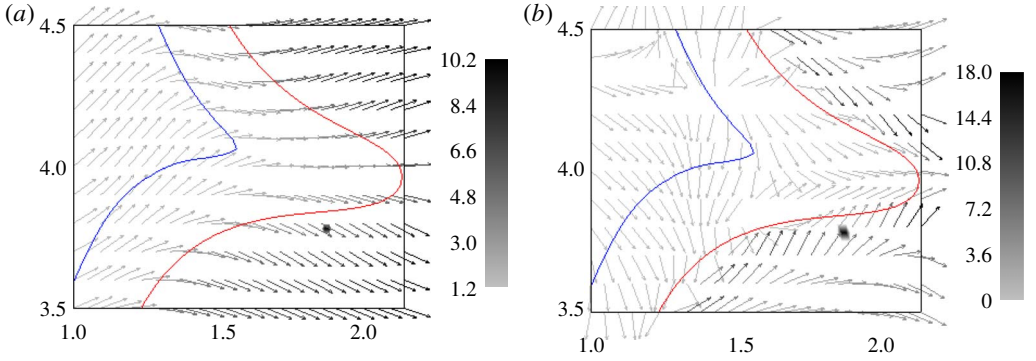

FIGURE 8. (Colour online) Two-dimensional fields of (*a*) velocity $\boldsymbol{u}$ and (*b*) pressure-induced acceleration $\rho^{-1}\boldsymbol{\nabla} p$. Arrows show the vector directions and the vector magnitudes are shown in grey scale. Left and right solid lines show the flamelet cold boundary and reaction surface, respectively. The fields are extrapolated to $y > 4$ mm using the symmetry boundary condition and are plotted in the transverse plane $z = z_A$ that point B and point A (black dot) lie on. The velocity is normalized using S_L, the density is normalized using ρ_u and the pressure gradient is normalized using $\rho_u(\sigma - 1)S_L^2/\delta_L$. Spatial distances x and y are reported in mm. Case H, $t = 18.3$ ms.

difference in u_B and u_A and, hence, a significant locally normal gradient of the locally tangential velocity appears, see dotted line in figure 7(*a*).

Furthermore, figure 6(*b*) shows that the local flamelet structure is perturbed in the vicinity of point A, e.g. the distance between the reaction surface and the cold boundary is increased. However, such effects are statistically weak, as discussed in detail elsewhere (Lipatnikov *et al.* 2018*c*).

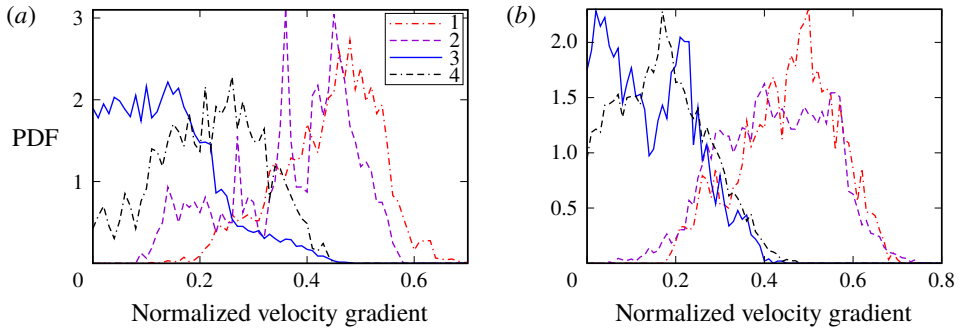

FIGURE 9. (Colour online) Conditioned PDFs of the absolute value of the gradient $\boldsymbol{n}\cdot\boldsymbol{\nabla}u$ of the axial velocity u in the direction normal to the local flamelet, evaluated at (a) $\langle c\rangle = 0.5$ and (b) $\langle c\rangle = 0.9$ in cases H ($\sigma = 7.53$, curves 1 and 2) and L ($\sigma = 2.50$, curves 3 and 4). The PDFs are obtained by sampling from points where either $0.97 < |n_y(\boldsymbol{x}, t)| \leqslant 0.99$ (curves 1 and 3) or $0.97 < |n_z(\boldsymbol{x}, t)| \leqslant 0.99$ (curves 2 and 4). The gradient is normalized using $|\boldsymbol{\nabla}u|_L = (\sigma - 1)S_L/\delta_L$.

It is also worth stressing that the local shear layers revealed by analysing the conditioned SFs in the present work and unburned mixture fingers studied by us earlier (Lipatnikov *et al.* 2015*a*, 2018*a*) are different phenomena and their appearances are controlled by different physical mechanisms. In particular, the local shear layer is a small-scale structure, which (i) is localized to flamelets, e.g. to a small neighbourhood of point A in figure 6(*a*), (ii) appears due to preferential acceleration of the reacting mixture and (iii) is observed in case H, but not in case L. The unburned mixture finger is (i) a large-scale structure, see the central part of figure 6(*b*), which (ii) appears due to acceleration of unburned gas by the axial pressure gradient induced due to combustion in surrounding flamelets and (iii) is observed both in cases H and L (Lipatnikov *et al.* 2015*a*, 2018*a*).

Finally, shown in figure 9 are conditioned probability density functions (PDFs) of the absolute value $|\boldsymbol{n}\cdot\boldsymbol{\nabla}u|$ of the gradient of the axial velocity u in the direction normal to the local flamelet. These conditioned PDFs were sampled within flamelets ($\epsilon < c(\boldsymbol{x}, t) \leqslant 1 - \epsilon$) and solely from points such that either $0.97 < |n_y(\boldsymbol{x}, t)| \leqslant 0.99$ or $0.97 < |n_z(\boldsymbol{x}, t)| \leqslant 0.99$. In other words, the PDFs were conditioned to flamelets that were almost normal to one of the transverse coordinate axes. Accordingly, these conditioned PDFs characterize the locally normal (to flamelets) gradient of the locally tangential velocity. Figure 9 indicates that the PDFs peak around $0.5|\boldsymbol{\nabla}u|_L$ in case H, see curves 1 and 2, where $|\boldsymbol{\nabla}u|_L = (\sigma - 1)S_L/\delta_L$ is the characteristic magnitude of velocity gradient in the laminar flame. Therefore, if flamelet zones characterized by either large $|n_y(\boldsymbol{x}, t)|$ (curves 1 and 3) or large $|n_z(\boldsymbol{x}, t)|$ (curves 2 and 4) are solely considered, then, the probability of finding a sufficiently large value of the locally normal gradient $\boldsymbol{n}\cdot\boldsymbol{\nabla}u$ of the locally tangential (either $|n_y(\boldsymbol{x}, t)|$ or $|n_z(\boldsymbol{x}, t)|$ is close to unity) velocity u is significant. In case L, see curves 3 and 4, such a probability is also substantial, but the PDFs are well shifted to the ordinate axis and peak around $0.2|\boldsymbol{\nabla}u|_L$ in spite of the fact that $|\boldsymbol{\nabla}u|_L$ applied to normalize the DNS data in case L is lower by a factor of approximately 8.7 than $|\boldsymbol{\nabla}u|_L$ in case H. Thus, comparison of the DNS data computed in cases H and L indicates that (i) the magnitude of the effect cannot simply be scaled invoking a characteristic of a laminar flame such as $|\boldsymbol{\nabla}u|_L$, but (ii) the effect stems from density variations, as the PDF shapes are clearly different in cases H and L.

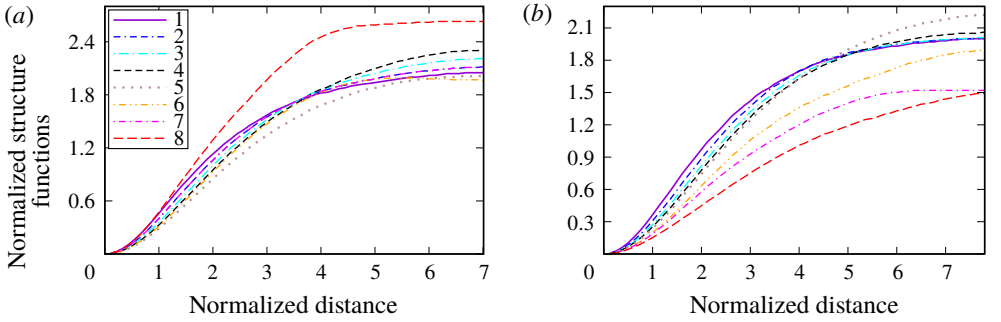

FIGURE 10. (Colour online) Longitudinal reactant–reactant SFs $D_{yz,L,uu}(x, r/\delta_\epsilon)$ normalized using $(v'^2 + w'^2)/2$ conditioned to the reactants. 1 – $x = 0.25$ mm, $\langle c\rangle = 0$; 2 – $x = 0.50$ mm, $\langle c\rangle = 0$; 3 – $x = 0.75$ mm, $\langle c\rangle = 0$; 4 – $x = 1.0$ mm, $\langle c\rangle = 0.001$; 5 – $x = 1.3$ or 1.4 mm in case H or L, respectively, $\langle c\rangle = 0.10$; 6 – $x = 1.5$ or 1.8 mm in case H or L, respectively, $\langle c\rangle = 0.25$; 7 – $x = 1.9$ or 2.3 mm in case H or L, respectively, $\langle c\rangle = 0.50$; 8 – $x = 2.5$ or 2.8 mm in case H or L, respectively, $\langle c\rangle = 0.75$.

To conclude this subsection, it is worth stressing that all data reported in figures 5–9 were only computed after the conditioned SFs had been analysed. In fact, diagnostic techniques required to obtain these data were developed, because the SF analysis implied the appearance of unexpected local flow structures and called for target-directed research into them. Therefore, the contents of the present subsection well illustrate the new opportunities offered by the conditioned SF approach.

4.3. *Turbulence in unburned reactants*

The conditioned SFs appear to be particularly useful for exploring the eventual effects of thermal expansion in premixed flames on the incoming turbulent flow of unburned reactants. This issue is of great fundamental importance, because a flame propagates into unburned reactants and, therefore, flame motion is controlled by its speed and the local velocity field in the unburned reactants just upstream of the flame. Although the aforementioned effects could be expected due to the appearance of combustion-induced pressure perturbations in the reactant turbulent flow, the effects have yet been poorly evidenced in experimental or DNS studies.

Application of the conditioned SFs to the present DNS data does evidence such effects. For instance, figure 10 shows the evolution of the longitudinal reactant–reactant SFs $D_{yz,L,uu}(x, r)$ upstream of and within the turbulent flame brushes in cases H and L. Upstream of the flame brushes, see curves 1–4, the evolution of $D_{yz,L,uu}(x, r)$ looks qualitatively and quantitatively similar in both cases. A decrease in $D_{yz,L,uu}(x, r)$ with x at $r/\delta_\epsilon < 3.5$, i.e. less-pronounced spatial variations in the velocity difference at larger x, could be attributed to an increase in the length scales of the spatially decaying turbulence. However, the behaviour of $D_{yz,L,uu}(x, r)$ in the H-flame brush, i.e. at $\langle c\rangle(x) \geqslant 0.1$, differs substantially from the behaviour of $D_{yz,L,uu}(x, r)$ in the L-flame brush, cf. curves 5–8 in figures 10(*a*) and 10(*b*), respectively. In particular, $D_{yz,L,uu}[\langle c\rangle(x), r/\delta_\epsilon]$ is increased and decreased with increasing $\langle c\rangle$ in cases H and L, respectively, with this difference between the two cases being well pronounced already at $\langle c\rangle(x) \geqslant 0.25$, cf. curves 6.

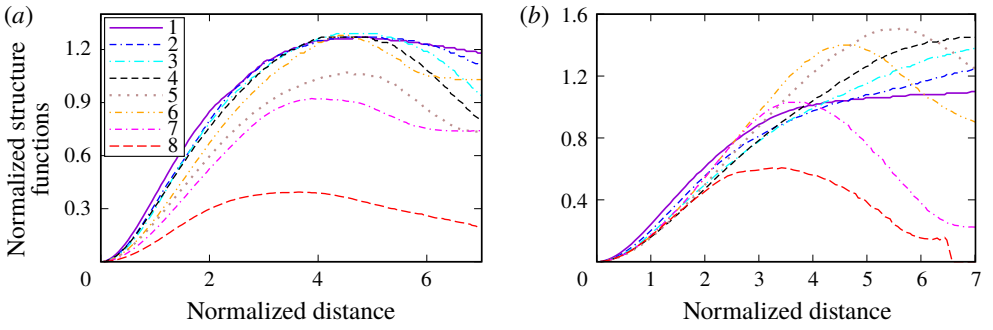

FIGURE 11. (Colour online) Longitudinal reactant–reactant SFs $D_{xx,L,uu}(x_A,\ r/\delta_\epsilon)$ normalized using u'^2 conditioned to the reactants. Legends are explained in caption to figure 10.

Figure 11 shows the evolution of the longitudinal reactant–reactant SFs $D_{xx,L,uu}(x_A, r)$ evaluated as follows

$$D_{xx,L,uu}(x,\ r) \equiv \langle [u_B(x_A + r,\ y,\ z,\ t) - \bar{u}_u(x_A + r,\ t) - u_A(x_A,\ y,\ z,\ t) + \bar{u}_u(x_A,\ t)]^2 I_{B,u} I_{A,u} \rangle / P_{uu}, \quad (4.1)$$

where $x_B = x_A + r,\ y_B = y_A,\ z_B = z_A$ and $\bar{u}_u(x,\ t)$ is the axial velocity conditionally averaged in the unburned gas over various y and z at instant t. Differences in the evolutions of $D_{xx,L,uu}(x,\ r)$ within the H and L flame brushes are also observed, but the effect is opposite to the effect documented for $D_{yz,L,uu}(x,\ r)$ in figure 10. Indeed, at small separation distances $r/\delta_\epsilon < 3$ in figure 11, $D_{xx,L,uu}(x,\ r)$ decreases with increasing $\langle c \rangle(x)$ in both cases, but the decrease is less pronounced in case L, characterized by a lower density ratio. Thus, figures 10 and 11 considered together indicate not only the influence of combustion-induced thermal expansion on the turbulent flow of constant-density unburned reactants, but also show that the influence is anisotropic.

Such differences between cases H and L are even more pronounced if the SFs $D_{yz,L,uu}(x,\ r/\delta_\epsilon)$ are 'compensated' by dividing them by reference SFs $D^*_{yz,L,uu} \equiv D_{yz,L,uu}(x = 0.25\ \text{mm},\ r/\delta_\epsilon)$, which are almost the same in cases H and L. Figure 12(*b*) (case L) shows that $D_{yz,L,uu}(x,\ r/\delta_\epsilon)/D^*_{yz,L,uu}$ decreases with distance x (or with $\langle c \rangle$) at small scales ($r/\delta_\epsilon < 4$). On the contrary, curves 5–8 in figure 12(*a*) (case H) show that $D_{yz,L,uu}(x,\ r/\delta_\epsilon)/D^*_{yz,L,uu}$ increases with increasing $\langle c \rangle$ provided that $r/\delta_\epsilon < 4$. Moreover, local maxima of $D_{yz,L,uu}(x,\ r/\delta_\epsilon)/D^*_{yz,L,uu}$ are observed at $r/\delta_\epsilon \approx 2.6$ and $\langle c \rangle(x^*) \approx 0.5$, see curve 7 in figure 12(*a*), or at $r/\delta_\epsilon \approx 4$ and $\langle c \rangle(x) \approx 0.75$, see curve 8. Furthermore, $D_{yz,L,uu}[\langle c \rangle(x) \approx 0.75,\ r/\delta_\epsilon]/D^*_{yz,L,uu}$ is larger than unity if $r/\delta_\epsilon > 1$ in case H. These results confirm that combustion-induced thermal expansion can substantially affect small-scale two-point velocity statistics even in the turbulent flow of constant-density unburned reactants.

Figure 13 shows another effect of this kind, i.e. differences between various compensated reactant–reactant SFs are substantially more pronounced at small scales ($r/\delta_\epsilon < 3$) in case H when compared to case L, thus, indicating that the influence of combustion-induced thermal expansion on the turbulence in unburned gas is highly anisotropic.

The influence of combustion on the incoming turbulent flow of constant-density reactants can also be evidenced using other methods. For instance, the present authors

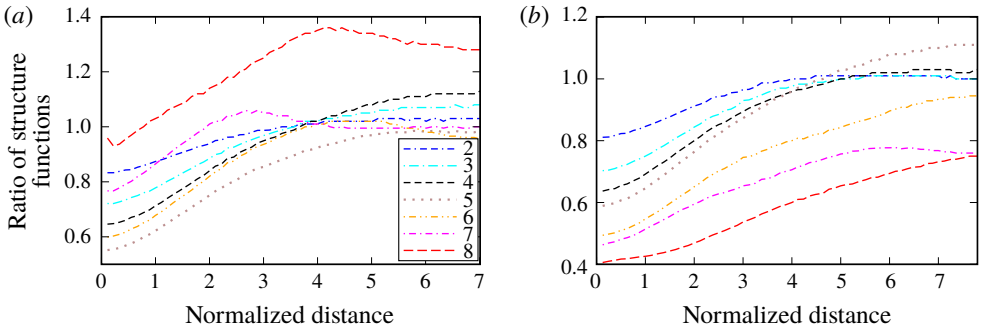

FIGURE 12. (Colour online) A ratio of the longitudinal reactant–reactant SFs $D_{yz,L,uu}(x,\, r/\delta_\epsilon)$ to a reference SF $D_{yz,L,uu}(x = 0.25 \text{ mm},\, r/\delta_\epsilon)$. Legends are explained in caption to figure 10.

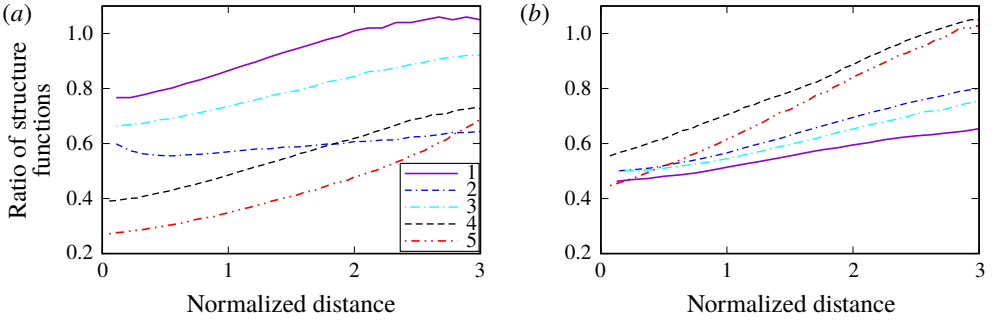

FIGURE 13. (Colour online) A ratio of reactant–reactant SFs to reference SFs obtained at $x = 0.25$ mm. 1 – Longitudinal SF $D_{yz,L,uu}$ for tangential velocities v and w; 2 – transverse SF $D_{xx,T,uu}$ for the axial velocity u; 3 – transverse SF $D_{yz,L,uu}$ for tangential velocities v and w, with $\boldsymbol{r}$ being equal to $\{0, 0, r\}$ and $\{0, r, 0\}$, respectively; 4 – longitudinal SF $D_{xx,L,uu}$ for the axial velocity u, defined with (4.1); 5 – transverse SF for tangential velocities v and w, with $\boldsymbol{r}$ being equal to $\{r, 0, 0\}$, i.e. $x_B = x_A + r$, $y_B = y_A$, and $z_B = z_A$.

(Lipatnikov *et al.* 2015*b*; Sabelnikov & Lipatnikov 2017) analysed the same DNS data in order to compare the behaviour of small-scale turbulence characteristics (i) upstream of the mean flame brushes H and L, (ii) at the leading points of the flame brushes at various t and (iii) at the unburned flamelet edges within the flame brushes. For these purposes, first, the flame leading point $\boldsymbol{x}_{lp}(t)$ was found by selecting the single grid point with the lowest axial coordinate x among all grid points characterized by $c(\boldsymbol{x}, t) \geqslant 0.05$ at each instant t. Subsequently, quantities conditioned to this point were evaluated by averaging their values over a small square located on the leading transverse plane $x = x_{lp}(t)$ and centred around the leading point $\boldsymbol{x}_{lp}(t)$. Second, due to the decay of incoming turbulence in the axial direction, quantities averaged over the leading transverse plane $x = x_{lp}(t)$ were considered to characterize turbulence upstream of the mean flame brush. Third, at each instant t, the unburned flamelet edge $x = x_f(y, z, t)$, i.e. a 2-D surface within the mean flame brush, was found using the following two constraints; (i) $c(x_i, y_j, z_k, t) \geqslant 0.05$ if $x_i = x_f(y_j, z_k, t)$, but (ii) $c(x_i, y_j, z_k, t) < 0.05$ if $x_i < x_f(y_j, z_k, t)$ at the same j and k. In other words, for each ray $\{j = \text{const.}, k = \text{const.}\}$ (or $\{y = \text{const.}, z = \text{const.}\}$) parallel to the x-axis, a single

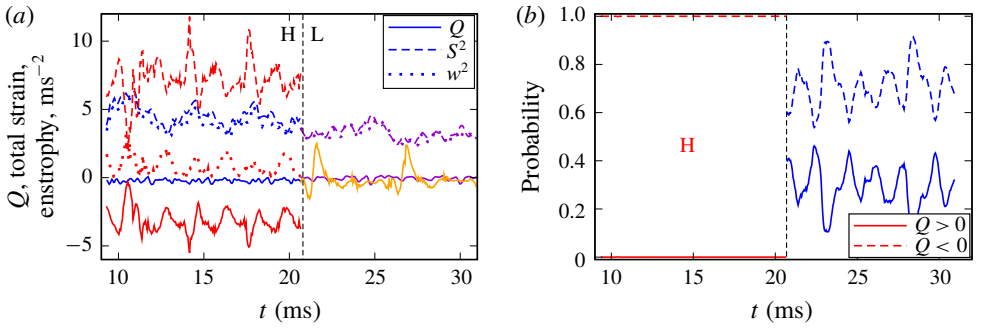

FIGURE 14. (Colour online) (*a*) Q criterion (solid lines), total strain $S^2/2$ (dashed lines) and enstrophy $\omega^2/4$ (dotted lines), averaged in the vicinity of the leading points $x_{lp}(t)$ (red and orange lines in cases H and L, respectively) and over leading planes $x = x_{lp}(t)$ (blue and violet lines in cases H and L, respectively). (*b*) Probabilities of $Q > 0$ (solid lines) and $Q < 0$ (dashed lines), conditioned to unburned flamelet edge, i.e. $c(\boldsymbol{x}, t) \approx 0.05$.

axial coordinate $x_i = x_f(y_j, z_k, t)$ was determined so that $c(x, y_j, z_k, t) < 0.05$ on the ray upstream of the unburned flamelet edge, but $c(x_i, y_j, z_k, t) \geqslant 0.05$ at the boundary. Then, the value of a considered quantity was averaged over the entire 2-D surface of the unburned flamelet edge $x_f(y, z, t)$ at different instants, i.e. over all $1 \leqslant j \leqslant 128$ and $1 \leqslant k \leqslant 128$ and over $t_{II} \leqslant t \leqslant t_{III}$. Thus, (i) characteristics of the incoming turbulence were averaged over the leading transverse plane $x = x_{lp}(t)$ upstream of the mean flame brush, (ii) characteristics of the leading point were averaged in its vicinity and (iii) characteristics of the unburned flamelet edge were averaged over a 2-D surface within the mean flame brush.

Three quantities, i.e. enstrophy $\omega^2 = (\boldsymbol{\nabla} \times \boldsymbol{u})^2$, total strain $S^2 = S_{ij}S_{ij}$ and the Q-criterion (Tsinober 2009)

$$Q = \tfrac{1}{4}\omega^2 - \tfrac{1}{2}S^2, \tag{4.2}$$

were studied to explore the influence of combustion-induced thermal expansion on small-scale turbulence by comparing their values averaged in the incoming turbulence with their values conditioned to either the leading point or to the unburned flamelet edge.

Figure 14(*a*) shows that the behaviour of ω^2, S^2 or Q averaged over the leading plane, i.e. in the incoming turbulent flow, is similar in cases H and L, cf. blue and violet lines. In both cases, the magnitudes of $\omega^2/4$ and $S^2/2$ are much larger than the magnitude of Q, which is predominantly negative. Moreover, in case L, the behaviour of Q averaged in the vicinity of the leading point is similar to the behaviour of Q averaged over the leading plane, cf. solid orange and violet lines. On the contrary, in case H characterized by a significantly larger density ratio, the behaviour of Q, ω^2 or S^2 averaged in the vicinity of the leading point differs significantly from the behaviour of Q, ω^2 or S^2, respectively, averaged over the leading plane, cf. red and blue lines. In particular, the former Q is always negative, see red solid line, thus, indicating a substantial influence of combustion-induced thermal expansion on small-scale turbulent structure in the unburned constant-density reactants. The negative values of Q averaged in the vicinity of the leading point imply that the potential flow perturbations caused by the thermal expansion overwhelm the rotational perturbations.

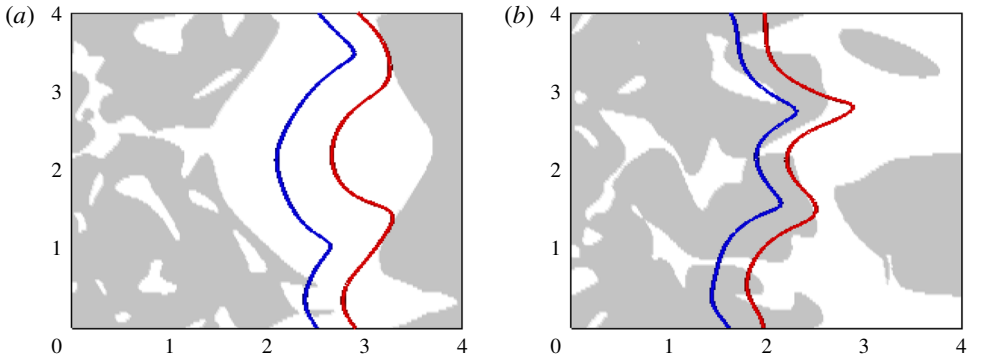

FIGURE 15. (Colour online) Typical 2-D images of the sign of the Q-criterion in cases (*a*) H and (*b*) L. Spatial regions characterized by $Q > 0$ and $Q < 0$ are shown in grey and white, respectively. Left and right solid lines show surfaces of $c(\boldsymbol{x}, t) \approx 0.01$ and $c(\boldsymbol{x}, t) \approx 0.5$, respectively. Spatial x and y coordinates are reported in mm, $z = 2$ mm.

In other words, the flow in the vicinity of the leading point appears to be significantly affected by pressure perturbations generated within flamelets.

Figure 14(*b*) reports probabilities of positive (solid lines) and negative (dashed lines) Q at the unburned flamelet edge $x = x_f(y, z, t)$. In case L, the probabilities of $Q < 0$ and $Q > 0$ are comparable. On the contrary, values of Q calculated at the unburned flamelet edge are negative in case H almost always, indicating a substantial influence of combustion-induced thermal expansion on small-scale turbulent structures in the unburned constant-density reactants. Again, the negative values of Q evaluated at the unburned flamelet edge imply that the flow upstream of the flamelets is significantly affected by pressure perturbations generated within the flamelets.

Typical 2-D images of the sign of the Q-criterion, plotted in figure 15, also indicate that $Q < 0$ in the vicinity of the flamelets in case H, but Q can change sign within the flamelets in case L.

Finally, it is worth noting that while figures 14 and 15 may appear to show the influence of combustion on the incoming turbulence in a clearer manner when compared to figures 10–13, the latter results convey additional information. In particular, contrary to the conditioned SFs, values of ω^2, S^2 or Q do not allow us to compare the magnitudes of the discussed effects at different length scales.

4.4. *Turbulence in heat-release zones*

SFs conditioned to HRZs, introduced in § 2.2, offer an opportunity to show the influence of combustion-induced thermal expansion on two-point statistics of the turbulent velocity field within such zones. If solely events such that the entire segment [A, B] is within the HRZ are selected, then, the probability of these events is low and decreases rapidly with distance r between the considered points A and B, see figure 16. Accordingly, statistically solid results can only be obtained at sufficiently small r. Nevertheless, the method does offer an opportunity to study behaviour of small-scale velocity differences in HRZs.

For instance, figure 17 indicates that the transverse SFs $D_{xx,T,ww}[\langle c\rangle(x), r/\delta_\epsilon]$ and $D_{yz,T,ww}[\langle c\rangle(x), r/\delta_\epsilon]$ differ significantly from one another at low r/δ_ϵ in case H, but exhibit similar dependencies on r/δ_ϵ in case L. In particular, at low r/δ_ϵ, the shape

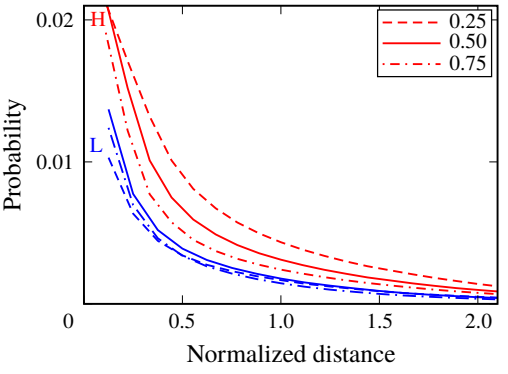

FIGURE 16. (Colour online) Probabilities of finding the entire segment [A, B] within HRZs ($0.75 < c(\boldsymbol{x}, t) < 0.95$), obtained at three different $\langle c\rangle(x)$ specified in the legend, versus the normalized segment length r/δ_ϵ. Red and blue lines show results obtained in cases H and L, respectively.

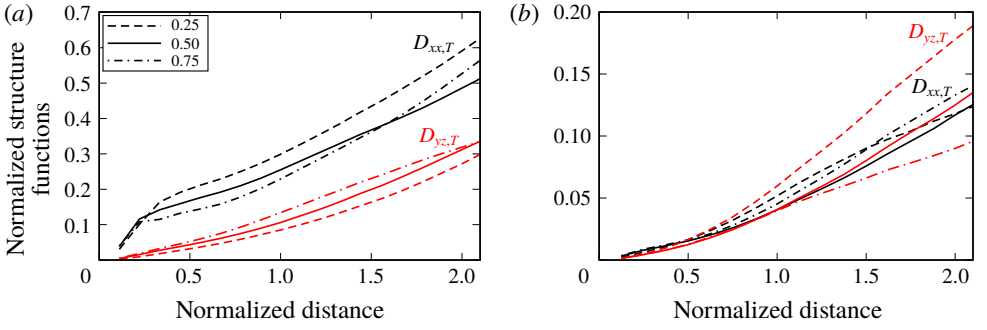

FIGURE 17. (Colour online) Transverse SFs $D_{xx,T,ww}[\langle c\rangle(x),\ r/\delta_\epsilon]$ (black lines) and $D_{yz,T,ww}[\langle c\rangle(x),\ r/\delta_\epsilon]$ (red lines) conditioned to HRZs ($0.75 < c(\boldsymbol{x}, t) < 0.95$) at three different $\langle c\rangle(x)$ specified in the legends. The SFs are normalized with u'^2 and $0.5(v'^2+w'^2)$, respectively, conditioned to the same zone at the same $\langle c\rangle$. (*a*) case H, (*b*) case L.

of the $D_{xx,T,ww}(r/\delta_\epsilon)$-curves in figure 17(*a*) differs significantly from the shape of the other curves.

The observed increase in $D_{xx,T,ww}[\langle c\rangle(x),\ r/\delta_\epsilon]$ at low r/δ_ϵ in case H may be associated with vorticity generation by baroclinic torque. Indeed, first, the present DNS data show that the components ω_y and ω_z of the vorticity vector $\boldsymbol{\nabla}\times\boldsymbol{u}$ are increased by baroclinic torque within the H-flame brush, whereas ω_x in case H and all three components of the vorticity vector in case L are decreased with increasing $\langle c\rangle$ due to dilatation (Lipatnikov *et al.* 2014, figure 2*b*). Second, variations in the axial velocity u in the transverse directions y and z, i.e. $D_{xx,T,ww}$, contribute to ω_z and ω_y, respectively, whereas variations in the tangential velocities v and w in the transverse directions z and y, respectively, i.e. $D_{yz,T,ww}$, contribute to ω_x. Consequently, (i) results plotted in figure 17(*a*) are in line with different behaviours of ω_y or ω_z (an increase with $\langle c\rangle$) and ω_x (a decrease with $\langle c\rangle$), reported in case H by Lipatnikov *et al.* (2014, figure 2*b*), and (ii) results plotted in figure 17(*b*) are in line with similar behaviours of ω_x, ω_y and ω_z, reported in case L by Lipatnikov *et al.* (2014, figure 2*b*). Accordingly, not only viscous dissipation and dilatation, but also baroclinic torque

may significantly affect small-scale turbulent eddies in flamelet preheat zones and the net effect (dissipation or generation of such eddies) depends on the conditions and is highly anisotropic. The conditioned SFs introduced in the present work appear to be an appropriate tool for exploring the competition of such mechanisms by analysing experimental or DNS data obtained under various conditions.

5. Conclusions

In order to explore the influence of combustion-induced thermal expansion on turbulent flow within a premixed flame brush, a new method for analysing DNS or experimental data is introduced. The method consists in conditioning the second-order structure functions of the velocity field to various events such as; (i) unburned reactants at both points, (ii) combustion products at both points, (iii) intermediate states of the mixture at both points, (iv) the reactants at one point and the products at another point, (v) the reactants at one point and an intermediate state at another point and (vi) the products at one point and an intermediate state at another point. Moreover, structure functions conditioned to heat-release zones are also introduced by considering events such that both points A and B are within the zones.

This method was applied to analysing DNS data obtained from two weakly turbulent premixed flames characterized by significantly different density ratios. Obtained results show that the conditioned SFs differ significantly from the mean SFs. Moreover, the SFs convey a large amount of important information on various local phenomena that stem from the influence of combustion-induced thermal expansion on turbulent flow, with the conditioned SFs not only showing well-studied phenomena, but also revealing less recognized and even new (to the best of the present authors' knowledge) phenomena.

In particular, the conditioned SFs indicate substantial and highly anisotropic influence of combustion-induced thermal expansion on turbulence in the incoming flow of constant-density unburned reactants, with the effect being also confirmed by exploring various small-scale characteristics of turbulence in the reactants, such as enstrophy, total strain and Q-criterion.

Moreover, the conditioned SFs reveal strong small-scale perturbations of the local velocity field, i.e. appearance of shear layers, within flamelets. This phenomenon was further confirmed by applying target-directed diagnostic techniques to analysing the DNS data, with the techniques being developed after revealing of the layers by analysing the conditioned SFs.

Furthermore, SFs conditioned to heat-release zones indicate a highly anisotropic influence of combustion-induced thermal expansion on the evolution of small-scale two-point velocity differences within flamelets, with the effect being opposite (an increase or a decrease) for different components of the local velocity vector.

The newly introduced conditioned SF method for analysing DNS or experimental data appears to be a promising research tool that deserves further development and application using both experiments and simulations. In particular, application of the method to analysing DNS data obtained at significantly different ratios of u'/S_L (and high Re_t) appears to be of great interest in order to determine the range of conditions such that results obtained by studying constant-density turbulence, e.g. the Kolmogorov theory, may be applied to turbulence within a premixed flame brush. While certain DNS data (Hamlington, Poludnenko & Oran 2011; Whitman *et al.* 2019) indicate that the influence of combustion-induced thermal expansion on turbulence in premixed flames is mitigated by u'/S_L, a domain of validity (if any) of

the Kolmogorov theory in premixed turbulent flames has not yet been outlined even for unburned reactants and this fundamental issue strongly challenges the combustion community.

It is also worth noting that the fact that substantially different results are obtained in two cases H and L, which are characterized by comparable $u'/S_L = O(1)$, but significantly different density ratios, implies that the Bray number $N_B \propto (\sigma - 1)S_L/u'$ (Bray 1995) is a more appropriate non-dimensional criterion for assessing the importance of the thermal-expansion effects (they are assumed to be of more importance at larger N_B), but this hypothesis requires further study.

Acknowledgements

V.A.S. gratefully acknowledges the financial support by ONERA and by the Ministry of Education and Science of the Russian Federation (Contract no. 14.G39.31.0001 of 13.02.2017). A.N.L. gratefully acknowledges the financial support by CERC and Chalmers Transport Area of Advance.

Appendix A. Exact transport equation for structure function conditioned to unburned reactants

While exact transport equations for the second-order SFs of the velocity field are well known in turbulence theory (Monin & Yaglom 1975; Hill 1997, 2001, 2002; Danaila *et al.* 1999; Antonia *et al.* 2003) since the pioneering study by Monin (1959), we are not aware on such equations for SFs conditioned to the fluid state. Since (i) the latter equations are substantially more complicated than the former and (ii) an analysis of the latter equations is beyond the focus of the present work, we will restrict ourselves to deriving an exact transport equation for the second-order SF tensor $D_{ij,uu}$, conditioned to fresh reactants, i.e. to $c(\boldsymbol{x}, t) < c_u \ll 1$ at two points $\boldsymbol{x}$ and $\boldsymbol{x}'$ (or $\boldsymbol{x}_A$ and $\boldsymbol{x}_B$, respectively, in the main body of the paper) connected by a vector $\boldsymbol{r} = \boldsymbol{x}' - \boldsymbol{x}$. Both derivation of the transport equations for $D_{ij,bb}$ or $D_{ij,ub}$ and the equations themselves are very similar to the case of $D_{ij,uu}$. Transport equations for $D_{ij,uf}$, $D_{ij,ff}$ or $D_{ij,bf}$ can be obtained using a basically similar method, but both the derivation and the equations are more cumbersome in these three cases and will not be addressed in the present appendix. It is worth noting that the case considered in the following, i.e. the transport equation for $D_{ij,uu}$, appears to be of the most fundamental interest, because combustion-induced thermal expansion should change the turbulence characteristics upstream of the flame and, in particular, $D_{ij,uu}$ in order to affect the speed of the flame propagation into the reactants and, therefore, the burning rate.

Let us derive transport equations for the conditioned second-order SFs of both total and fluctuating velocity fields while solely the former SFs are addressed in the main body of the paper. For brevity, both (total and fluctuating) velocity vectors will be designated using the same symbol $\boldsymbol{u} = \{u_1, u_2, u_3\}$, but terms that vanish in the equations for the former (total) field will be specified when necessary. Moreover, the subscript u will be skipped for brevity, because the following analysis is restricted to reactants.

Since the density of the fresh reactants is considered to be constant, i.e. $\rho(\boldsymbol{x}, t) = \rho_u$, the continuity and Navier–Stokes equations read

$$\frac{\partial u_k}{\partial x_k} = -\frac{\partial U_k}{\partial x_k} \tag{A 1}$$

and

$$\frac{\partial u_i}{\partial t} + (U_k + u_k)\frac{\partial u_i}{\partial x_k} = -\frac{1}{\rho_u}\frac{\partial p}{\partial x_i} + \frac{\partial \tau_{ik}}{\partial x_k} - u_k\frac{\partial U_i}{\partial x_k} + a_i, \tag{A 2}$$

respectively, for both fields. Here,

$$\tau_{ik} = \nu \left(\frac{\partial u_i}{\partial x_k} + \frac{\partial u_k}{\partial x_i} \right) \tag{A 3}$$

is the fluctuating viscous stress tensor and

$$a_i = - \left(\frac{\partial U_i}{\partial t} + U_k \frac{\partial U_i}{\partial x_k} + \frac{1}{\rho_u} \frac{\partial P}{\partial x_i} \right) + \nu \frac{\partial}{\partial x_k} \left(\frac{\partial U_i}{\partial x_k} + \frac{\partial U_k}{\partial x_i} \right) \tag{A 4}$$

is the acceleration term. If symbols u_i and p are associated with the total velocity and pressure fields, respectively, then, $U_i = P = a_i = 0$. If symbols u_i and p are associated with the fluctuating velocity and pressure fields, respectively, then, $U_i = \langle \hat{u}_i I_u \rangle / \langle I_u \rangle$ and $P = \langle \hat{p} I_u \rangle / \langle I_u \rangle$ designate the ith component of the velocity vector and pressure, respectively, conditioned to the reactants, whereas $\hat{u}_i$ and $\hat{p}$ refer to the total velocity and pressure fields, respectively, in this case.

It is worth stressing that neither the divergence $\nabla \cdot \boldsymbol{U}$ nor the acceleration a_i vanishes, because a statistical sub-ensemble over which a conditional average is taken depends on $\boldsymbol{x}$ and t due to the random motion of an interface that bounds the reactants. Consequently, taking the conditional average does not commute with taking the time or spatial derivative (Libby 1975; Townsend 1976; Kuznetsov & Sabelnikov 1990) and extra terms averaged over a surface $c(\boldsymbol{x}, t) = \text{const.}$ that separates two fluid states (e.g. unburned reactants and burned products in the simplest case of self-propagation of an infinitely thin flame front) appear in the conditioned transport equations (Kataoka 1986), as will be shown later. Such surface-averaged terms describe exchange of mass, momentum or energy between the two fluid states and fundamentally change features of the conditioned fields when compared to conventional mean fields. For instance, as shown by Libby (1975), the divergence of a conditioned velocity does not vanish even in a constant-density flow.

To derive transport equations for the instantaneous second-order SFs $d_{ij} = (u_i' - u_i)(u_j' - u_j) \equiv v_i v_j$, a method developed by Hill (2001, 2002) is used. Henceforth, q and q' designate values of an arbitrary (scalar, vector or tensor) quantity q, taken at points $\boldsymbol{x}$ and $\boldsymbol{x}'$, respectively, and symbol v_i designates the difference $u_i' - u_i$. First, (A 2) written for u_i is subtracted from (A 2) written for u_i'. Second, the obtained equation is recast to a transport equation for v_i using (A 1) and considering $\boldsymbol{x}$ and $\boldsymbol{x}'$ to be independent variables. Third, the equation for v_i (v_j) is multiplied with v_j (v_i, respectively) and the two equations are added. Since details of the derivation of a similar transport equation are presented by Hill (2002), we restrict ourselves to reporting the final result. In the considered case, it involves some extra terms, e.g. the conditioned velocities $\boldsymbol{U}$ and $\boldsymbol{U}'$, and reads

$$\begin{aligned} &\frac{\partial d_{ij}}{\partial t} + (U_k + u_k) \frac{\partial d_{ij}}{\partial x_k} + (U_k' + u_k') \frac{\partial d_{ij}}{\partial x_k'} \\ &\quad = G_{ij} - \pi_{ij} + q_{ij} - (\varepsilon_{ij}' + \varepsilon_{ji}') - (\varepsilon_{ij} + \varepsilon_{ji}) + v_j (a_i' - a_i) + v_i (a_j' - a_j), \end{aligned} \tag{A 5}$$

where

$$G_{ij} = -u_k' v_j \frac{\partial U_i'}{\partial x_k'} - u_k' v_i \frac{\partial U_j'}{\partial x_k'} + u_k v_j \frac{\partial U_i}{\partial x_k} + u_k v_i \frac{\partial U_j}{\partial x_k}, \tag{A 6}$$

$$\pi_{ij} = \frac{\partial v_j \delta p}{\partial x_i'} + \frac{\partial v_j \delta p}{\partial x_i} + \frac{\partial v_i \delta p}{\partial x_j'} + \frac{\partial v_i \delta p}{\partial x_j} - \delta p \left(\frac{\partial v_j}{\partial x_i'} + \frac{\partial v_j}{\partial x_i} + \frac{\partial v_i}{\partial x_j'} + \frac{\partial v_i}{\partial x_j} \right), \tag{A 7}$$

$$q_{ij} = \frac{\partial v_j \tau'_{ik}}{\partial x'_k} - \frac{\partial v_j \tau_{ik}}{\partial x_k} + \frac{\partial v_i \tau'_{jk}}{\partial x'_k} - \frac{\partial v_i \tau_{jk}}{\partial x_k}, \tag{A 8}$$

$$\varepsilon'_{ij} = \tau'_{ik}\frac{\partial u'_j}{\partial x'_k}, \quad \varepsilon_{ij} = \tau_{ik}\frac{\partial u_j}{\partial x_k}, \tag{A 9a,b}$$

and $\delta p = p' - p$. If d_{ij} is associated with the total velocity field, then, $U_k = U'_k = G_{ij} = a_i = a'_i = 0$.

To obtain transport equations for conditioned SFs defined by (2.12), let us begin with multiplication of (A 5) with a product $I(\boldsymbol{x}, t)I'(\boldsymbol{x}', t)$ of two indicator functions taken at points $\boldsymbol{x}$ and $\boldsymbol{x}'$, respectively. If, following Kataoka (1986), the indicator function is defined as follows

$$I(\boldsymbol{x}, t) = H[c_u - c(\boldsymbol{x}, t)], \tag{A 10}$$

where H is Heaviside function, then,

$$\begin{aligned}\frac{\partial I}{\partial t} &= -\frac{\partial c}{\partial t}\delta[c_u - c(\boldsymbol{x}, t)] = \left[(U_k + u_k)\frac{\partial c}{\partial x_k} - S_d|\nabla c|\right]\delta[c_u - c(\boldsymbol{x}, t)] \\ &= -[(U_k + u_k)n_k + S_d]|\nabla c|\delta[c_u - c(\boldsymbol{x}, t)] = -[(U_k + u_k)n_k + S_d]\Sigma,\end{aligned} \tag{A 11}$$

$$\frac{\partial I}{\partial x_k} = -\frac{\partial c}{\partial x_k}\delta[c_u - c(\boldsymbol{x}, t)] = n_k\Sigma, \tag{A 12}$$

and

$$\frac{\partial I}{\partial t} + (U_k + u_k)\frac{\partial I}{\partial x_k} = -S_d\Sigma, \tag{A 13}$$

where $\delta[c_u - c(\boldsymbol{x}, t)]$ is the Dirac delta function, $\boldsymbol{n} = -\nabla c/|\nabla c|$ is the unit vector normal to an interface of $c(\boldsymbol{x}, t) = c_u$, which separates fresh reactants from reacting mixture, $\Sigma = |\nabla c|\delta[c_u - c(\boldsymbol{x}, t)]$ is the interface surface density, the so-called displacement speed S_d is the speed of propagation of the interface of $c(\boldsymbol{x}, t) = c_u$ with respect to the reactants. Equations (A 11), (A 12) and (A 13) are well known both in the multiphase flow (Kataoka 1986; Drew & Passman 2006) and combustion (Im *et al.* 2004) literature. In the combustion case, $S_d = [\nabla \cdot (\rho D\nabla c) + W]/(\rho|\nabla c|)$, where D is the molecular diffusivity of c and W is the mass rate of product creation. At the interface of $c(\boldsymbol{x}, t) = c_u \ll 1$, the rate W vanishes and $S_d = [\nabla \cdot (\rho D\nabla c)/(\rho|\nabla c|)]_{c=c_u}$. If, at $c = c_u$, flamelets retain the structure of the unperturbed laminar flame, then, $S_d = S_L$.

Let us use (A 12) and (A 13) to transform some terms in an equation that results from multiplication of (A 5) with a product of II'. First, since I does not depend on $\boldsymbol{x}'$ and I' does not depend on $\boldsymbol{x}$,

$$\begin{aligned}&II'\left[\frac{\partial d_{ij}}{\partial t} + (U_k + u_k)\frac{\partial d_{ij}}{\partial x_k} + (U'_k + u'_k)\frac{\partial d_{ij}}{\partial x'_k}\right] \\ &= \frac{\partial}{\partial t}(II'd_{ij}) + (U_k + u_k)\frac{\partial}{\partial x_k}(II'd_{ij}) + (U'_k + u'_k)\frac{\partial}{\partial x'_k}(II'd_{ij}) \\ &\quad - I'd_{ij}\left[\frac{\partial I}{\partial t} + (U_k + u_k)\frac{\partial I}{\partial x_k}\right] - Id_{ij}\left[\frac{\partial I'}{\partial t} + (U'_k + u'_k)\frac{\partial I'}{\partial x'_k}\right] \\ &= \frac{\mathrm{D}}{\mathrm{D}t}(II'd_{ij}) + (I'S_d\Sigma + IS'_d\Sigma')d_{ij},\end{aligned} \tag{A 14}$$

where

$$\frac{\mathrm{D}}{\mathrm{D}t} \equiv \frac{\partial}{\partial t} + (U_k + u_k)\frac{\partial}{\partial x_k} + (U'_k + u'_k)\frac{\partial}{\partial x'_k}. \tag{A 15}$$

Second, similarly,

$$II'\pi_{ij} = \pi^*_{ij} - v_j\delta p(In'_i\Sigma' + I'n_i\Sigma) - v_i\delta p(In'_j\Sigma' + I'n_j\Sigma), \tag{A 16}$$

where

$$\begin{aligned}\pi^*_{ij} \;=\; & \frac{\partial}{\partial x'_i}(II'v_j\delta p) + \frac{\partial}{\partial x_i}(II'v_j\delta p) + \frac{\partial}{\partial x'_j}(II'v_i\delta p) + \frac{\partial}{\partial x_j}(II'v_i\delta p) \\ & - II'\delta p\left(\frac{\partial v_j}{\partial x'_i} + \frac{\partial v_j}{\partial x_i} + \frac{\partial v_i}{\partial x'_j} + \frac{\partial v_i}{\partial x_j}\right).\end{aligned} \tag{A 17}$$

Third, similarly,

$$II'q_{ij} = q^*_{ij} - v_j(I\tau'_{ik}n'_k\Sigma' - I'\tau_{ik}n_k\Sigma) - v_i(I\tau'_{jk}n'_k\Sigma' - I'\tau_{jk}n_k\Sigma), \tag{A 18}$$

where

$$q^*_{ij} = \frac{\partial}{\partial x'_k}(II'v_j\tau'_{ik}) - \frac{\partial}{\partial x_k}(II'v_j\tau_{ik}) + \frac{\partial}{\partial x'_k}(II'v_i\tau'_{jk}) - \frac{\partial}{\partial x_k}(II'v_i\tau_{jk}). \tag{A 19}$$

Thus, (A 5) reads

$$\begin{aligned}\frac{\mathrm{D}}{\mathrm{D}t}(II'd_{ij}) \;=\; & -\pi^*_{ij} + q^*_{ij} + II'[G_{ij} - (\varepsilon'_{ij} + \varepsilon'_{ji}) - (\varepsilon_{ij} + \varepsilon_{ji}) + v_j(a'_i - a_i) + v_i(a'_j - a_j)] \\ & - (I'S_d\Sigma + IS'_d\Sigma')d_{ij} + v_j\delta p(In'_i\Sigma' + I'n_i\Sigma) + v_i\delta p(In'_j\Sigma' + I'n_j\Sigma) \\ & - v_j(I\tau'_{ik}n'_k\Sigma' - I'\tau_{ik}n_k\Sigma) - v_i(I\tau'_{jk}n'_k\Sigma' - I'\tau_{jk}n_k\Sigma),\end{aligned} \tag{A 20}$$

where π^*_{ij} and q^*_{ij} are given by (A 17) and (A 19), respectively. If d_{ij} is associated with the total velocity field, then, $U_i = U'_i = G_{ij} = a_i = a'_i = 0$.

Let us change independent variables $\boldsymbol{x}$ and $\boldsymbol{x}'$ to new independent variables $\boldsymbol{X} = (\boldsymbol{x} + \boldsymbol{x}')/2$ and $\boldsymbol{r} = \boldsymbol{x}' - \boldsymbol{x}$ (Monin 1959; Hill 1997, 2001, 2002; Danaila *et al.* 1999; Antonia *et al.* 2003). Then,

$$\left.\begin{aligned}\frac{\partial}{\partial x_k} &= \frac{1}{2}\frac{\partial}{\partial X_k} - \frac{\partial}{\partial r_k}, \quad & \frac{\partial}{\partial x'_k} &= \frac{1}{2}\frac{\partial}{\partial X_k} + \frac{\partial}{\partial r_k}, \\ \frac{\partial}{\partial x'_k} - \frac{\partial}{\partial x_k} &= 2\frac{\partial}{\partial r_k}, \quad & \frac{\partial}{\partial x'_k} + \frac{\partial}{\partial x_k} &= \frac{\partial}{\partial X_k}.\end{aligned}\right\} \tag{A 21}$$

Consequently, since $u_k = (u_k + u'_k - v_k)/2$ and $u'_k = (u_k + u'_k + v_k)/2$,

$$\frac{\partial}{\partial x_k}(II'u_kd_{ij}) + \frac{\partial}{\partial x'_k}(II'u'_kd_{ij}) = \frac{1}{2}\frac{\partial}{\partial X_k}[II'(u_k + u'_k)d_{ij}] + \frac{\partial}{\partial r_k}(II'd_{ijk}), \tag{A 22}$$

where $d_{ijk} = v_iv_jv_k$. Similarly,

$$\frac{\partial}{\partial x_k}(II'U_kd_{ij}) + \frac{\partial}{\partial x'_k}(II'U'_kd_{ij}) = \frac{1}{2}\frac{\partial}{\partial X_k}[II'(U_k + U'_k)d_{ij}] + \frac{\partial}{\partial r_k}(II'V_kd_{ij}), \tag{A 23}$$

where $V_k = U'_k - U_k$. Thus,

$$\frac{\mathrm{D}}{\mathrm{D}t}(II'd_{ij}) = \frac{\partial}{\partial t}(II'd_{ij}) + \frac{\partial}{\partial X_k}\left(II'\frac{U'_k+u'_k+U_k+u_k}{2}d_{ij}\right) + \frac{\partial}{\partial r_k}(II'd_{ijk}) + \frac{\partial}{\partial r_k}(II'V_k d_{ij}). \tag{A 24}$$

If d_{ij} is associated with the total velocity field, then, $U_k = U'_k = V_k = 0$.

Moreover,

$$\pi^*_{ij} = \frac{\partial}{\partial X_i}(II'v_j\delta p) + \frac{\partial}{\partial X_j}(II'v_i\delta p) - II'\delta p\left(\frac{\partial v_i}{\partial X_j} + \frac{\partial v_j}{\partial X_i}\right). \tag{A 25}$$

Furthermore,

$$\begin{aligned} q^*_{ij} &= \frac{1}{2}\frac{\partial}{\partial x'_k}[II'v_j(\tau'_{ik}+\tau_{ik}+\tau'_{ik}-\tau_{ik})] - \frac{1}{2}\frac{\partial}{\partial x_k}[II'v_j(\tau'_{ik}+\tau_{ik}-\tau'_{ik}+\tau_{ik})] \\ &\quad + \frac{1}{2}\frac{\partial}{\partial x'_k}[II'v_i(\tau'_{jk}+\tau_{jk}+\tau'_{jk}-\tau_{jk})] - \frac{1}{2}\frac{\partial}{\partial x_k}[II'v_i(\tau'_{jk}+\tau_{jk}-\tau'_{jk}+\tau_{jk})] \\ &= \frac{\partial}{\partial r_k}[II'v_j(\tau'_{ik}+\tau_{ik})] + \frac{1}{2}\frac{\partial}{\partial X_k}[II'v_j(\tau'_{ik}-\tau_{ik})] \\ &\quad + \frac{\partial}{\partial r_k}[II'v_i(\tau'_{jk}+\tau_{jk})] + \frac{1}{2}\frac{\partial}{\partial X_k}[II'v_i(\tau'_{jk}-\tau_{jk})]. \end{aligned} \tag{A 26}$$

Thus, (A 20) holds if its left-hand side, π^*_{ij}, and q^*_{ij} are given by (A 24), (A 25) and (A 26), respectively. For brevity, terms G_{ij}, ε_{ij}, and a_i are written using the original variables, i.e. $\boldsymbol{x}$ and $\boldsymbol{x}'$, see (A 6), (A 9) and (A 4), respectively. If d_{ij} is associated with the total velocity field, then, $U_i = U'_i = G_{ij} = a_i = a'_i = 0$.

Ensemble-averaged (A 20) reads

$$\begin{aligned} &\underbrace{\frac{\partial}{\partial t}(P_{uu}D_{ij,uu})}_{T_1} + \underbrace{\frac{\partial}{\partial X_k}\left(\frac{U'_k+U_k}{2}P_{uu}D_{ij,uu}\right)}_{T_2} + \underbrace{\frac{\partial}{\partial X_k}\left\langle II'\frac{u'_k+u_k}{2}d_{ij}\right\rangle}_{T_3} + \underbrace{\frac{\partial}{\partial r_k}(V_kP_{uu}D_{ij,uu})}_{T_4} \\ &+ \underbrace{\frac{\partial}{\partial r_k}(P_{uu}D_{ijk,uu})}_{T_5} = \underbrace{\left\langle II'\left(-u'_kv_j\frac{\partial U'_i}{\partial x'_k} - u'_kv_i\frac{\partial U'_j}{\partial x'_k} + u_kv_j\frac{\partial U_i}{\partial x_k} + u_kv_i\frac{\partial U_j}{\partial x_k}\right)\right\rangle}_{T_6} \\ &\underbrace{-\frac{\partial}{\partial X_i}\langle II'v_j\delta p\rangle - \frac{\partial}{\partial X_j}\langle II'v_i\delta p\rangle + \left\langle II'\delta p\left(\frac{\partial v_i}{\partial X_j}+\frac{\partial v_j}{\partial X_i}\right)\right\rangle}_{T_7} \\ &+ \underbrace{\frac{\partial}{\partial r_k}\langle II'[v_j(\tau'_{ik}+\tau_{ik})+v_i(\tau'_{jk}+\tau_{jk})]\rangle + \frac{\partial}{\partial X_k}\left\langle II'\left(v_j\frac{\tau'_{ik}-\tau_{ik}}{2}+v_i\frac{\tau'_{jk}-\tau_{jk}}{2}\right)\right\rangle}_{T_8} \\ &\underbrace{-\langle II'(\varepsilon'_{ij}+\varepsilon'_{ji}+\varepsilon_{ij}+\varepsilon_{ji})\rangle}_{T_9} + \underbrace{\langle II'[v_j(a'_i-a_i)+v_i(a'_j-a_j)]\rangle}_{T_{10}} \\ &\underbrace{-\langle(I'S_d\Sigma + IS'_d\Sigma')d_{ij}\rangle}_{T_{11}} + \underbrace{\langle v_j\delta p(In'_i\Sigma' + I'n_i\Sigma) + v_i\delta p(In'_j\Sigma' + I'n_j\Sigma)\rangle}_{T_{12}} \\ &\underbrace{-\langle v_j(I\tau'_{ik}n'_k\Sigma' - I'\tau_{ik}n_k\Sigma) + v_i(I\tau'_{jk}n'_k\Sigma' - I'\tau_{jk}n_k\Sigma)\rangle}_{T_{13}}, \end{aligned} \tag{A 27}$$

where $P_{uu} = \langle II' \rangle$ is the probability of finding fresh reactants at points $\boldsymbol{x}$ and $\boldsymbol{x}'$, $D_{ij,uu} = \langle II' d_{ij} \rangle / \langle II' \rangle$ is the second-order SF tensor conditioned to the reactants, $d_{ij} = v_i v_j$ is the instantaneous second-order SF tensor, $v_i = u_i' - u_i$, $V_i = U_i' - U_i$, $\delta p = p' - p$, the acceleration a_i and the dissipation ε_{ij} are given by (A 4) and (A 9), respectively, and, in terms T_{11}, T_{12} and T_{13}, products that involve Σ are evaluated at the interface of $c(\boldsymbol{x}, t) = c_u$. If the SFs d_{ij} and $D_{ij,uu}$ are associated with the total velocity field, then $U_i = V_i = a_i = 0$ and terms T_2, T_4, T_6 and T_{10} vanish.

The derived transport equation describes the distribution of the flow kinetic energy over various scales. If d_{ij} and $D_{ij,uu}$ are associated with the fluctuating velocity field, the structure of the equation is partly similar to the structure of the transport equation for turbulent kinetic energy (Monin & Yaglom 1975; Pope 2000). In particular, T_1 is an unsteady term, the linear term T_2 and term T_3 describe convection of $D_{ij,uu}$ by the conditionally mean flow and the turbulent transport of the energy, respectively, in $\boldsymbol{X}$-space, the linear term T_4 is associated with redistribution of the energy in $\boldsymbol{r}$-space, i.e. between eddies of different length scales, due to the conditionally mean flow, T_5 involves conditioned third-order SFs $P_{uu} D_{ijk,uu} = \langle II' d_{ijk} \rangle$ and describes nonlinear redistribution of the energy in $\boldsymbol{r}$-space due to the turbulence, T_6 and T_{10} describe production of the turbulent energy due to non-uniformities of the conditionally mean flow, T_7 is the turbulent transport and redistribution of the energy due to pressure fluctuations, T_8 is the viscous transport term and T_9 describes viscous dissipation of the turbulent energy.

Terms T_{11}, T_{12} and T_{13} are specific to conditioned transport equations. The known exact transport equations for SFs (Hill 2002) do not involve such terms, while similar terms appear in the transport equation for turbulent kinetic energy conditioned to fresh reactants at a single point (Im *et al.* 2004). These surface-averaged terms describe exchange of energy between the two fluid states and fundamentally change the features of conditioned fields when compared to conventional mean fields. For instance, these terms make mean and conditioned SFs significantly different, cf. results shown in dotted and other lines in figures 1–3.

Finally, it is worth noting that terms T_2, T_3, T_4, T_5, T_7 and T_8 are written using coordinates $\boldsymbol{X}$ and $\boldsymbol{r}$ in order to obtain a common structure of the left-hand side, as discussed above, whereas other terms are written in coordinates $\boldsymbol{x}$ and $\boldsymbol{x}'$. Nevertheless, the use of two different sets of coordinates does not seem to impede evaluating all the terms by analysing DNS data. This will be a subject for future work.

REFERENCES

ANTONIA, R. A., SMALLEY, R. J., ZHOU, T., ANSELMET, F. & DANAILA, L. 2003 Similarity of energy structure functions in decaying homogeneous isotropic turbulence. *J. Fluid Mech.* **487**, 245–269.

ASPDEN, A. J., DAY, M. S. & BELL, J. B. 2016 Three-dimensional direct numerical simulation of turbulent lean premixed methane combustion with detailed kinetics. *Combust. Flame* **165**, 266–283.

BALLAL, D. R. 1979 The structure of premixed turbulent flames. *Proc. R. Soc. Lond.* A **367**, 353–380.

BRAY, K. N. C. 1995 Turbulent transport in flames. *Proc. R. Soc. Lond.* A **451**, 231–256.

BRAY, K. N. C., CHAMPION, M., LIBBY, P. A. & SWAMINATHAN, N. 2011 Scalar dissipation and mean reaction rates in premixed turbulent combustion. *Combust. Flame* **158**, 2017–2022.

CHAUDHURI, S., KOLLA, H., DAVE, H. L., HAWKES, E. R., CHEN, J. H. & LAW, C. K. 2017 Flame thickness and conditional scalar dissipation rate in a premixed temporal turbulent reacting jet. *Combust. Flame* **184**, 273–285.

DANAILA, L., ANSELMET, F., ZHOU, T. & ANTONIA, R. A. 1999 Similarity of energy structure functions in decaying homogeneous isotropic turbulence. *J. Fluid Mech.* **391**, 359–372.

DAVIDSON, P. A. 2015 *Turbulence: An Introduction for Scientists and Engineers*, 2nd edn. Oxford University Press.

DREW, D. A. & PASSMAN, S. L. 2006 *Theory of Multicomponent Fluids*. Springer.

DRISCOLL, J. F. 2008 Turbulent premixed combustion: flamelet structure and its effect on turbulent burning velocities. *Prog. Energy Combust. Sci.* **34**, 91–134.

FRISCH, U. 1995 *Turbulence: The Legacy of A. N. Kolmogorov*. Cambridge University Press.

FURUKAWA, J., NOGUCHI, Y. & HIRANO, T. 2000 Investigation of flame generated turbulence in a large-scale and low-intensity turbulent premixed flame with a 3-element electrostatic probe and a 2-D LDV. *Combust. Sci. Technol.* **154**, 163–178.

FURUKAWA, J., NOGUCHI, Y., HIRANO, T. & WILLIAMS, F. A. 2002 Anisotropic enhancement of turbulence in large-scale, low-intensity turbulent premixed propane-air flames. *J. Fluid Mech.* **462**, 209–243.

FURUKAWA, J., OKAMOTO, K. & HIRANO, T. 1996 Turbulence characteristics within the local reaction zone thickness of a high-intensity turbulent premixed flame. *Proc. Combust. Inst.* **26**, 405–412.

GÖKALP, I., SHEPHERD, I. G. & CHENG, R. K. 1988 Spectral behavior of velocity fluctuations in premixed turbulent flames. *Combust. Flame* **71**, 313–323.

GÜNTHER, R. 1983 Turbulence properties of flames and their measurement. *Prog. Energy Combust. Sci.* **9**, 105–154.

HAMLINGTON, P. E., POLUDNENKO, A. Y. & ORAN, E. S. 2011 Interactions between turbulence and flames in premixed reacting flows. *Phys. Fluids* **23**, 125111.

HILL, R. J. 1997 Applicability of Kolmogorov's and Monin's equations of turbulence. *J. Fluid Mech.* **353**, 67–81.

HILL, R. J. 2001 Equations relating structure functions of all orders. *J. Fluid Mech.* **434**, 379–388.

HILL, R. J. 2002 Exact second-order structure-function relationships. *J. Fluid Mech.* **468**, 317–326.

IM, Y. H., HUH, K. Y., NISHIKI, S. & HASEGAWA, T. 2004 Zone conditional assessment of flame-generated turbulence with DNS database of a turbulent premixed flame. *Combust. Flame* **137**, 478–488.

KADOWAKI, S. & HASEGAWA, T. 2005 Numerical simulation of dynamics of premixed flames: flame instability and vortex–flame interaction. *Prog. Energy Combust. Sci.* **31**, 193–241.

KARLOVITZ, B., DENNISTON, D. W. & WELLS, F. E. 1951 Investigation of turbulent flames. *J. Chem. Phys.* **19**, 541–547.

KATAOKA, I. 1986 Local instant formulation of two-phase flow. *Intl J. Multiphase Flow* **12**, 745–758.

KIM, J., BASSENNE, M., TOWERY, C. A. Z., HAMLINGTON, P. E., POLUDNENKO, A. Y. & URZAY, J. 2018 The cross-scale physical-space transfer of kinetic energy in turbulent premixed flames. *J. Fluid. Mech.* **848**, 78–116.

KOLLA, H., HAWKES, E. R., KERSTEIN, A. R., SWAMINATHAN, N. & CHEN, J. H. 2014 On velocity and reactive scalar spectra in turbulent premixed flames. *J. Fluid Mech.* **75**, 456–487.

KOLMOGOROV, A. N. 1941 The local structure of turbulence in incompressible viscous fluid for very large Reynolds number. *Dokl. Akad. Nauk SSSR* **30**, 299–303.

KUZNETSOV, V. R. 1982 Limiting laws of propagation of a turbulent flame. *Combust. Explos. Shock Waves* **18**, 172–179.

KUZNETSOV, V. R. & SABELNIKOV, V. A. 1990 *Turbulence and Combustion*. Hemisphere.

LANDAU, L. D. & LIFSHITZ, E. M. 1987 *Fluid Mechanics*. Pergamon Press.

LAPOINTE, S. & BLANQUART, G. 2016 Fuel and chemistry effects in high Karlovitz premixed turbulent flames. *Combust. Flame* **167**, 294–307.

LESIEUR, M., MÉTAIS, O. & COMTE, P. 2005 *Large-Eddy Simulations of Turbulence*. Cambridge University Press.

LIBBY, P. A. 1975 On the prediction of intermittent turbulent flows. *J. Fluid Mech.* **68**, 273–295.

LIBBY, P. A. & BRAY, K. N. C. 1981 Countergradient diffusion in premixed turbulent flames. *AIAA J.* **19**, 205–213.

LIPATNIKOV, A. N. 2009 Can we characterize turbulence in premixed flames? *Combust. Flame* **156**, 1242–1247.

LIPATNIKOV, A. N. & CHOMIAK, J. 2010 Effects of premixed flames on turbulence and turbulent scalar transport. *Prog. Energy Combust. Sci.* **36**, 1–102.

LIPATNIKOV, A. N., CHOMIAK, J., SABELNIKOV, V. A., NISHIKI, S. & HASEGAWA, T. 2015*a* Unburned mixture fingers in premixed turbulent flames. *Proc. Combust. Inst.* **35**, 1401–1408.

LIPATNIKOV, A. N., CHOMIAK, J., SABELNIKOV, V. A., NISHIKI, S. & HASEGAWA, T. 2015*b* Influence of heat release in a premixed flame on weakly turbulent flow of unburned gas: a DNS study. In *25th International Colloquium on Dynamics of Explosions and Reactive Systems.* ICDERS.

LIPATNIKOV, A. N., CHOMIAK, J., SABELNIKOV, V. A., NISHIKI, S. & HASEGAWA, T. 2018*a* A DNS study of the physical mechanisms associated with density ratio influence on turbulent burning velocity in premixed flames. *Combust. Theor. Model.* **22**, 131–155.

LIPATNIKOV, A. N., NISHIKI, S. & HASEGAWA, T. 2014 A direct numerical simulation study of vorticity transformation in weakly turbulent premixed flames. *Phys. Fluids* **26**, 105104.

LIPATNIKOV, A. N., NISHIKI, S. & HASEGAWA, T. 2015*c* DNS assessment of relation between mean reaction and scalar dissipation rates in the flamelet regime of premixed turbulent combustion. *Combust. Theor. Model.* **19**, 309–328.

LIPATNIKOV, A. N., NISHIKI, S. & HASEGAWA, T. 2019 A DNS assessment of linear relations between filtered reaction rate, flame surface density, and scalar dissipation rate in a weakly turbulent premixed flame. *Combust. Theor. Model.* (in press).

LIPATNIKOV, A. N., SABELNIKOV, V. A., CHAKRABORTY, N., NISHIKI, S. & HASEGAWA, T. 2018*b* A DNS study of closure relations for convection flux term in transport equation for mean reaction rate in turbulent flow. *Flow Turbul. Combust.* **100**, 75–92.

LIPATNIKOV, A. N., SABELNIKOV, V. A., NISHIKI, S. & HASEGAWA, T. 2017 Flamelet perturbations and flame surface density transport in weakly turbulent premixed combustion. *Combust. Theor. Model.* **21**, 205–227.

LIPATNIKOV, A. N., SABELNIKOV, V. A., NISHIKI, S. & HASEGAWA, T. 2018*c* Combustion-induced local shear layers within premixed flamelets in weakly turbulent flows. *Phys. Fluids* **30**, 085101.

LIPATNIKOV, A. N., SABELNIKOV, V. A., NISHIKI, S. & HASEGAWA, T. 2018*d* Does flame-generated vorticity increase turbulent burning velocity? *Phys. Fluids* **30**, 081702.

LIPATNIKOV, A. N., SABELNIKOV, V. A., NISHIKI, S., HASEGAWA, T. & CHAKRABORTY, N. 2015*d* DNS assessment of a simple model for evaluating velocity conditioned to unburned gas in premixed turbulent flame. *Flow Turbul. Combust.* **94**, 513–526.

MATALON, M. 2007 Intrinsic flame instabilities in premixed and nonpremixed combustion. *Annu. Rev. Fluid Mech.* **39**, 163–191.

MONIN, A. S. 1959 The theory of locally isotropic turbulence. *Dokl. Akad. Nauk SSSR* **125**, 515–518.

MONIN, A. S. & YAGLOM, A. M. 1975 *Statistical Fluid Mechanics: Mechanics of Turbulence*, vol. 2. MIT Press.

MURA, A., ROBIN, V., CHAMPION, M. & HASEGAWA, T. 2009 Small scale features of velocity and scalar fields in turbulent premixed flames. *Flow Turbul. Combust.* **82**, 339–358.

MURA, A., TSUBOI, K. & HASEGAWA, T. 2008 Modelling of the correlation between velocity and reactive scalar gradients in turbulent premixed flames based on DNS data. *Combust. Theor. Model.* **12**, 671–698.

NISHIKI, S., HASEGAWA, T., BORGHI, R. & HIMENO, R. 2002 Modeling of flame-generated turbulence based on direct numerical simulation databases. *Proc. Combust. Inst.* **29**, 2017–2022.

NISHIKI, S., HASEGAWA, T., BORGHI, R. & HIMENO, R. 2006 Modelling of turbulent scalar flux in turbulent premixed flames based on DNS databases. *Combust. Theor. Model.* **10**, 39–55.

O'BRIEN, J., TOWERY, C. A. Z., HAMLINGTON, P. E., IHME, M., POLUDNENKO, A. Y. & URZAY, J. 2017 The cross-scale physical-space transfer of kinetic energy in turbulent premixed flames. *Proc. Combust. Inst.* **36**, 1967–1975.

OBUKHOV, A. M. 1941 The spectral energy distribution in a turbulent flow. *Dokl. Akad. Nauk SSSR* **32** (1), 22–24.

POINSOT, T., VEYNANTE, D. & CANDEL, S. 1991 Quenching processes and premixed turbulent combustion diagrams. *J. Fluid Mech.* **228**, 561–606.

POPE, S. B. 2000 *Turbulent Flows*. Cambridge University Press.

RENARD, P.-H., THÉVENIN, D., ROLON, J. C. & CANDEL, S. 2000 Dynamics of flame/vortex interactions. *Prog. Energy Combust. Sci.* **26**, 225–282.

ROBERTS, W. L., DRISCOLL, J. F., DRAKE, M. C. & GOSS, L. P. 1993 Images of the quenching of a flame by vortex – to quantify regimes of turbulent combustion. *Combust. Flame* **94**, 58–69.

ROBIN, V., MURA, A. & CHAMPION, M. 2011 Direct and indirect thermal expansion effects in turbulent premixed flames. *J. Fluid Mech.* **689**, 149–182.

ROBIN, V., MURA, A., CHAMPION, M. & HASEGAWA, T. 2010 Modeling of the effects of thermal expansion on scalar turbulent fluxes in turbulent premixed flames. *Combust. Sci. Technol.* **182**, 449–464.

SABELNIKOV, V. A. & LIPATNIKOV, A. N. 2017 Recent advances in understanding of thermal expansion effects in premixed turbulent flames. *Annu. Rev. Fluid Mech.* **49**, 91–117.

SABELNIKOV, V. A., LIPATNIKOV, A. N., CHAKRABORTY, N., NISHIKI, S. & HASEGAWA, T. 2016 A transport equation for reaction rate in turbulent flows. *Phys. Fluids* **28**, 081701.

SABELNIKOV, V. A., LIPATNIKOV, A. N., CHAKRABORTY, N., NISHIKI, S. & HASEGAWA, T. 2017 A balance equation for the mean rate of product creation in premixed turbulent flames. *Proc. Combust. Inst.* **36**, 1893–1901.

SABELNIKOV, V. A., LIPATNIKOV, A. N., NISHIKI, S. & HASEGAWA, T. 2019 Application of conditioned structure functions to exploring influence of premixed combustion on two-point turbulence statistics. *Proc. Combust. Inst.* **37**, 2433–2441.

SCURLOCK, A. C. & GROVER, J. H. 1953 Propagation of turbulent flames. *Proc. Combust. Inst.* **4**, 645–658.

TOWERY, C. A. Z., POLUDNENKO, A. Y., URZAY, J., O'BRIEN, J., IHME, M. & HAMLINGTON, P. E. 2016 Spectral kinetic energy transfer in turbulent premixed reacting flows. *Phys. Rev.* E **93**, 053115.

TOWNSEND, A. A. 1976 *The Structure of Turbulent Shear Flow*, 2nd edn. Cambridge University Press.

TSINOBER, A. 2009 *An Informal Conceptual Introduction to Turbulence*. Springer.

URANAKARA, H. A., CHAUDHURI, S., DAVE, H. L., ARIAS, P. G. & IM, H. G. 2016 A flame particle tracking analysis of turbulence–chemistry interaction in hydrogen–air premixed flames. *Combust. Flame* **163**, 220–240.

VIDETO, B. D. & SANTAVICCA, D. A. 1990 Flame–turbulence interactions in a freely-propagating, premixed flame. *Combust. Sci. Technol.* **70**, 47–73.

WABEL, T. M., SKIBA, A. W. & DRISCOLL, J. F. 2018 Evolution of turbulence through a broadened preheat zone in a premixed piloted Bunsen flame from conditionally-averaged velocity measurements. *Combust. Flame* **188**, 13–27.

WANG, H., HAWKES, E. R., CHEN, J. H., ZHOU, B., LI, Z. & ALDÉN, M. 2017 Direct numerical simulations of a high Karlovitz number laboratory premixed jet flame – an analysis of flame stretch and flame thickening. *J. Fluid Mech.* **815**, 511–536.

WHITMAN, S. H. R., TOWERY, C. A. Z., POLUDNENKO, A. Y. & HAMLINGTON, P. E. 2019 Scaling and collapse of conditional velocity structure functions in turbulent premixed flames. *Proc. Combust. Inst.* **37**, 2527–2535.